UNIVERSITÀ DEGLI STUDI FIRENZE

DIEF – Dipartimento di Ingegneria Industriale

PhD School: Energetica e Tecnologie Industriali e Ambientali Innovative

Academic Discipline (SSD) ING-IND/09

EFFECT OF NATURAL GAS COMPOSITION ON THE OPERATION OF LOW NO_X BURNERS IN COMBUSTION CHAMBER FOR HEAVY-DUTY GAS TURBINE

PhD Candidate:	Ing. Serena Romano
Academic Tutor	Prof. Antonio Andreini
Industrial Supervisor	Dr. Ing. Giovanni Riccio
Industrial Supervisor	Dr. Ing. Roberto Meloni
PhD School Coordinator	Prof. Giampaolo Manfrida

PhD School Cycle: XXXIII (2017/2020)

Abstract

Modern heavy-duty gas turbines employ lean-premixed combustion system to meet more and more strict emission regulations. The development of such combustion technology with low emissions and stable operation in an increasingly wide range of operating conditions requires a deep understanding of the mechanisms that affect the combustion performance or even the operability of the entire gas turbine.

Furthermore, gas turbine manufacturers are tasked increasingly with expanding operational fuel flexibility, due to the relative wide range of natural gas composition supplies, the increased demand from Oil&Gas customers to burn gas with notable higher hydrocarbons (C_2+) content and considering the potential addition of hydrogen to the natural gas infrastructure in the next future; therefore the impact of gas composition on gas turbine operability and combustion related aspects it is a matter of several studies.

This work aims to address the impact of natural gas composition, observed during an experimental test campaign of a lean premixed annular combustor for heavy-duty gas turbine, on both emissions and flame stability with focus on natural gas blends containing a certain level of ethane and hydrogen.

For this purpose, Large Eddy Simulations (LES) of an annular combustor sector equipped with a partially-premixed burner are carried out at relevant pressure and temperature for three different natural gas compositions. An extended approach of the Zimont TCF model that includes the combined effects of strain rate and heat loss on the flame brush modelling has been implemented resulting in a more adequate description of flame shape, thermal field and extinction phenomena with respect to standard model, thus improving the predictive accuracy of CFD analysis that can be used since the preliminary design phase of

combustion systems. Indeed, an accurate tool capable to predict fuel composition effects would reduce expensive tests on prototypes.

Such novel approach has been used to investigate NO_X emission and lean blow off (LBO) showing promising results and good accuracy compared against available experimental data.

Contents

List of Figures

List of Tables

Nomenclature

Letters

a	Flame strain rate	[1/s]
A	Model constant	[-]
c	Progress variable	[-]
$C_s\Delta$	Length scale of sub-grid turbulence	[m]
D	Molecular diffusivity	[m^2/s]
Da	Damkohler	[-]
Ea	Activation Energy	[-]
G	Stretch factor	[-]
κ	Flame stretch	[1/s]
h	Enthalpy	[J/kg]
k	Turbulent kinetic energy	[m^2/s^2]
Ka	Karlovitz number	[-]
Ma	Markstein number	[-]
L_t	Turbulent integral length scale	[-]
Le	Lewis Number	[-]
n	Flame front normal	[-]
p	Pressure	[Pa]
P_s	Pilot split	[%]
P_{s0}	Reference pilot split	[%]

Pr	Prandlt Number	[-]
Q	Heat release	[W/m3]
R	Specidic gas costant	[-]
Re	Reynold Number	[-]
Sc	Schimdt Number	[-]
S_c	Consumption speed	[m/s]
S_{ij}	Fluid strain rate	[1/s]
S_l	Laminar flame speed	[m/s]
S_t	Turbulent flame speed	[m/s]
T	Temperature	[K]
T_a	Operating temperature	[°C]
T_{a0}	Reference operating temperature	[°C]
u	Velocity	[m/s]
ν_{sgs}	Sub-grid velocity	[m/s]
z	Mixture fraction	[-]
Ze	Zeldovich Number	[-]
u'_Δ	Turbulent velocity fluctuation	[m/s]
Y	Species mass fraction	[-]

Symbols

α	Thermal diffusivity	[m^2/s]
β	Heat loss coefficient	[-]
Δ	Filter length	[m]
δ_{ij}	Kronecker delta	[-]
δ_L^0	Laminar flame front thickness	[m]

ε	Turbulent kinetic energy dissipation	[m^2/s^3]
ν	Kinematic viscosity	[m^2/s]
ϕ	Equivalence ratio	[-]
Γ_k	Efficiency function	[-]
σ_c	Flame front curvature	[1/s]
$\dot{\omega}_c$	Progress variable source	[kg/m^3s]
ρ	Density	[kg/m^3]
∇	Gradient operator	[-]
ψ	Heat loss correction parameter	[-]

Subscripts

ad	Adiabatic condition
b	Burnt
cr	Critic
F	Fuel
mod	Modelled
res	Resolved
sgs	Sub-grid
u	Unburnt

Acronyms

CDC	Compressor Discharge Chamber
CFD	Computational Fluid Dynamics
C_2+	Hydrocarbons with two or more carbon atoms

DLE	Dry Low Emission
DNS	Direct Numerical Simulation
ETFC	Extended Turbulent Flame Closure
FAR	Full Annular Rig
FGM	Flamelet Generated Manifold
GT	Gas Turbine
ISO	International Standards Organization
LBO	Lean Blow-out
LES	Large Eddy Simulation
LHV	Lower Heating value
LNG	Liquified Natural Gas
MWI	Modified Wobbe Index
NS	Navier Stokes
OEM	Original Equipment Manufacturer
PCD	Pressure Compressore Discharge
RANS	Reynold Average Navier Stokes
RMS	Root Mean Squares
SG	Specific Gravity
TCD	Temperature Compressore Discharge
TFC	Turbulent Flame Closure

1 Introduction

In all the energy scenarios considered up to 2040, world energy demand will rise by more than 1% each year driven by increasing prosperity mainly in fast-growing developing economies [1]. The primary energy demand trend is shown in *Figure 1.1* in terms of fuel consumption, focusing on a scenario which assumes that government policies, technology and social preferences continue to evolve in a manner and speed seen over the recent past [2].

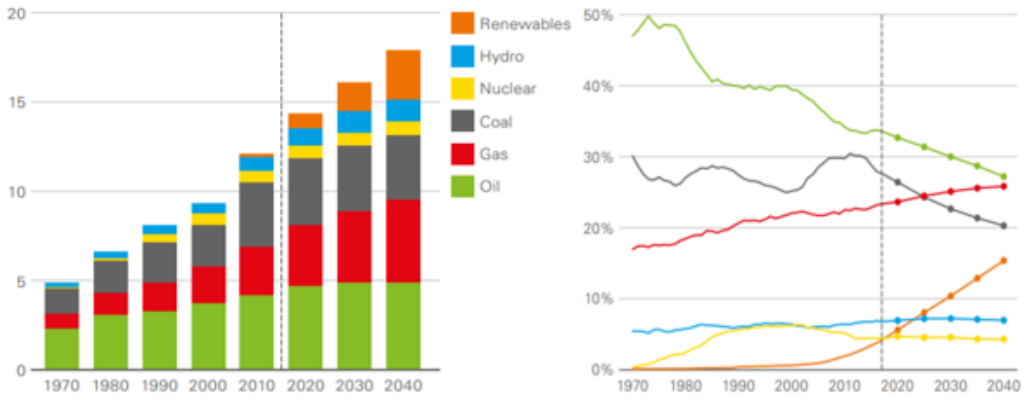

***Figure 1.1**: Primary energy consumption by fuel in Billion toe [1]*

One of the biggest challenges of our time is to meet rising energy demand while reducing emissions at the same time and limiting environmental impact. In this scenario, natural gas plays a significant role in satisfying the energy need worldwide while helping to mitigate the risks of climate change. Indeed, natural gas is the only fossil fuel for which

predicted demand in 2040 is higher than today, and it will become the largest fuel in the global energy mix. By 2040, projections state that natural gas will continue to supply around 30 percent of global energy and the demand will grow robustly led by industry and power sector, also supported by the continuing expansion of liquefied natural gas (LNG) [2], *Figure 1.2.*

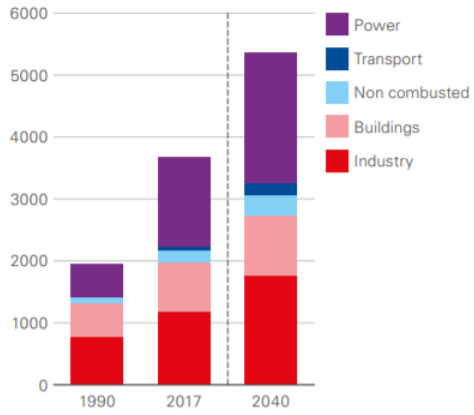

***Figure 1.2**: Natural gas consumption in Bcm [2]*

In this context, gas turbines still play a significant role in Oil&Gas sector and remain a key technology in the electric power generation as well as in the industrial sector being an attractive choice for new plants because of its efficiency. However, gas turbine manufacturers are called in a challenging development of fuel-flexible combustors capable of operating with variable fuel gases, due to the relative wide range of natural gas composition supplies within the distribution system and to meet more and more challenging requests from the Oil&Gas market to be capable of accepting a wider range of fuel gas compositions (LNG, alternative, refinery...), while producing very low emissions. To meet the increasingly stringent environmental regulation requirements about emissions, lean premixed combustion systems are adopted for low emissions gas turbine operation. Due to the complexity of these combustion systems, whose operation is requested to be optimized for a large range of operating conditions minimizing the emissions, the fuel gas

composition variability has an important effect on the performance of a lean-premixed natural gas-fired gas turbine system.

The challenges in the flexible fuel adaptation are related to the properties of the fuel mixtures that can change significantly limiting the engine operability when more and more restrictive laws must be respected.

Despite natural gas is mainly associated to methane, its constituents may vary with the extraction process utilized and the location from which it is extracted. Generally, such gases contain methane between 60–99%, ethane between 0–20%, and some other higher-order hydrocarbons (C_2+) in smaller quantities along with traces of carbon dioxide, hydrogen sulfide, nitrogen and rare gases [3]. As an example, *Table 1.1* and *Table 1.2* show the typical composition worldwide of natural gas and LNG produced [4].

	CH_4	C_2H_6	C_3+	N_2	CO_2
Algeria	85.70	7.10	2.42	4.27	0.36
Lybia	86.47	9.81	0.94	0.81	1.88
Norway	90.10	4.82	1.48	2.34	1.23
Russia	97.62	0.98	0.46	0.83	0.10
US	95.7	3.0	0.8	0.2	0.3

***Table 1.1**: Typical composition worldwide of natural gas*

	CH_4	C_2H_6	C_3+	N_2	CO_2
Algeria	91.4	7.35	0.62	0.63	0
Lybia	81.39	12.44	4.15	2.02	0
Nigeria	91.70	5.52	2.75	0.03	0
Australia	86.26	8.23	4.25	1.26	0
Norway	92.03	5.75	1.76	0.46	0
Russia	92.54	4.47	2.92	0.07	0
US	99.7	0.09	0.04	0.17	0

***Table 1.2**: Typical composition worldwide of LNG*

Furthermore, as the energy system progressively decarbonize and renewable energy sources are expected to contribute increasingly to electricity generation, the excess of electricity during times of peak will be converted into hydrogen and the addition of

hydrogen to the natural gas grid as an energy storage vector presents an operating scenario to be considered for GT OEMs and power generators. Several projects around the world are already injecting hydrogen into natural gas grids.

Indeed, the natural gas composition variation can lead to different reaction mechanisms having an impact on combustion performance or even on the operability of the entire gas turbine: of particular concern is the effect of fuel composition on combustor NO_X emissions, blowout, flashback and dynamic stability, that may be adversely affected [5].
The reaction rate and the flame propagation speed through a fuel/air mixture are dependent on the mixture composition, changing in burning velocity may strongly influence the tendency of the gas turbine burners to blowout or flashback. An increased reaction rate will help extend the lean blow-out (LBO) limits, similarly to adding ethane or hydrogen to natural gas. Also, change in fuel composition affects the level of combustion dynamic (the oscillations of the pressure typical of premixed combustion) and hardware durability. Furthermore, it might be expected that the effect of gas composition plays a significant role on NO_X formation pathways [6].
According to the above, it is fundamental to understand how a given combustor operability will be affected by fuel composition variability.

It is worth to mention that some limitations to gas composition variability is common practice to control the thermal input to the gas turbine combustor. Such a practice acts in limiting the variation of the Modified Wobbe Index (MWI), Eq.(1.1).

$$\mathrm{MWI} = \frac{\mathrm{LHV}}{\sqrt{\mathrm{SG}_{gas} \times \mathrm{T}_{gas}}} \tag{1.1}$$

Where LHV is the Lower Heating Value, SG_{gas} is the Specific gravity relative to air and T_{gas} is the absolute temperature of the gas fuel.

MWI gives a measure of the energy input provided to the combustion system, since fuels having similar MWI provide the same heat input with similar fuel injection pressure need. Usually, for a specific combustion system's design, MWI variations within ±5% from value corresponding to the design fuel composition do not require to modify the size of

fuel injection holes, while larger MWI variations often imply some major modifications to the combustion and fuel supply systems. Three species are the main actors of the MWI variation, *Figure 1.3*:

- Higher Order Hydrocarbons: C_2+
- Hydrogen: H_2
- Inerts: in particular N_2 and CO_2

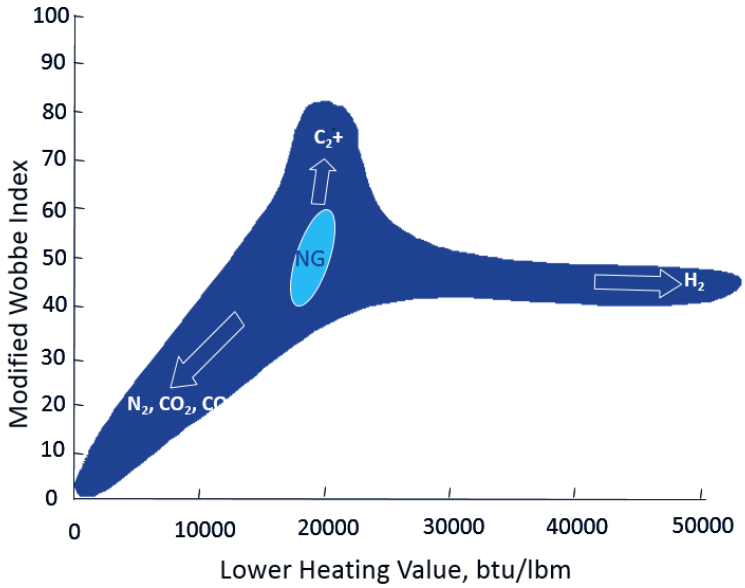

***Figure 1.3**: MWI-LHV diagramm*

Nevertheless, for natural gas compositions even having the same MWI, studies show that turbulent flame speed, chemical kinetics, heat release rate, diffusivity and flame strain rate, can vary evidently affecting the operability of lean premixed combustor systems [7].

Gas turbine combustion system can be particularly sensitive to C_2+ content: results of experimental test campaigns of an annular combustor for heavy-duty gas turbine show the effect of different fuel mixture of methane and C_2H_6 on both emissions and flame stability [8]. CH_4/C_2H_6 fuel blends, even for modest amount of ethane, increase the blowout margin allowing to operate with lower operating temperature and pilot fuel split, reaching a global reduction of NO_X emissions while keeping pressure pulsations under control as well as preserving enough margin to blow-out with respect to a mixture of pure methane.

1.1 State of the Art

This research area, dedicated to the study of natural gas blends, is currently a field of fundamentals experiments and modelling, although there are very limited public available data regarding the impacts of varying fuel composition on the operation of DLE turbines [5]. In addition, the published data often exist over a range of pressure and temperature that do not allow making more definitive conclusions about composition impact [9].

As described above, the fuel composition directly affects many combustion properties. These properties include heat release rate, burning velocity, autoignition tendencies, adiabatic flame temperature and can directly affect gas turbine operation, as the combustors have been designed for specific tolerances. Key operability issues are briefly introduced below:

- NO_X emissions are tangible affected by composition, the addition of higher hydrocarbons cause the additional NO_X for a given combustor temperature, on the contrary the change in natural gas composition has little effect on the production of CO from the gas turbine. Flores et al. [10] studied the effects of gas composition on emissions in a pre-mixed, swirl-stabilized combustor testing four fuels mixture of methane, ethane and propane and they noted that the fuel composition did have an effect on fuel mixing, which could have led to hot spots in the combustor and potentially high NO_X as a result, further highlighting the effect of the pilot fuel line on emissions. In 2000, Lee [11] looked at NO_X emissions for several hydrocarbon fuels, including methane, ethane, and propane documenting a non-linear increase in NO_X production for pure fuels as the carbon-to-hydrogen ratio of the fuel is increased. Similar outcomes are obtained by Hack and McDonell [12].
- Blowout refers to situations where the flame becomes detached from the location where it is anchored and is physically “blown out” of the combustor. Changes in operating conditions or fuel composition can cause the flame to locally blow off of one stabilization location and stabilize in another. These local blowoff events

are generally quite abrupt and lead to discontinuous changes in emissions, and combustion dynamics with slight changes in operating conditions. Higher hydrocarbons and hydrogen extend blowoff boundaries, due to their elevated flame speeds related to methane. Extensive work by Santavicca [13] [14] shown that fuel composition influences combustion instability limits by changing the flame length. For example, increasing the percentage of ethane or hydrogen in a fuel will increase the flame speed and therefore decrease the flame length. Similar data and points have been made by Russ et al. [15] and Richards et al. [16], that compared the phase of the flame response of a forced flame excited by vortical instabilities, and showed that the variation in phase of the response with fuel (for CH_4, C_2H_6,) could be interpreted as a difference in time delay which directly correlated with the differing flame speeds, and therefore flame lengths.

- Flashback occurs when the turbulent flame speed exceeds the flow velocity along some streamline, allowing the flame to propagate upstream into premixing section. Fuel species that lead to an increase of flame speed are therefore the maximum contributors to this phenomenon; in particular high amount of C_2+ and H_2 can be very critical. According to this definition it is considered as one of the most challenging operational issues when hydrogen, or high hydrogen content fuels, are burnt; the reason is related to the very high flame speeds typical of these fuels.
- Combustion instability refers to damaging pressure oscillations associated with oscillations in the combustion heat release rate. These oscillations cause wear and damage to combustor components and, in extreme cases, can cause liberation of pieces into the hot gas path, damaging downstream turbine components. Combustion instability can also initiate other operability issues such as flashback or blowout.

All of the above processes are generally strong functions of various kinetic properties of the fuel and, as such, have some (but quite different) sensitivities to fuel composition.

All the results show that important conclusions about fuel sensitivity can be determined from flame speed, given the importance in controlling reaction mechanisms. Ethane increases the laminar flame speed relative to methane [17] as reported in *Figure 1.4*.

Hydrogen has an effect even more significant [18]; *Figure 1.5* shows the laminar flame speed as hydrogen is added to the mixture of methane in the indicated percentages.

While low hydrogen percentages (~10%) only lead to a small percentage increase in laminar flame speed, the flame speed rises rapidly with hydrogen addition at higher levels of hydrogen.

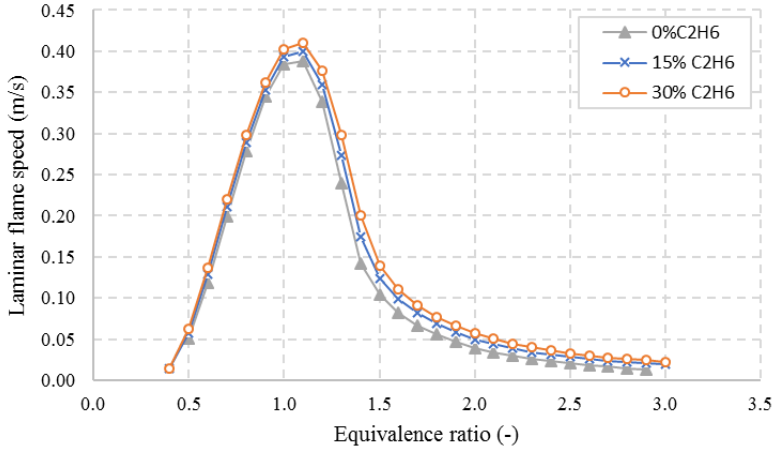

***Figure 1.4**: Laminar flame speed of methane-ethane air flames, at ambient temperature and atmospheric pressure*

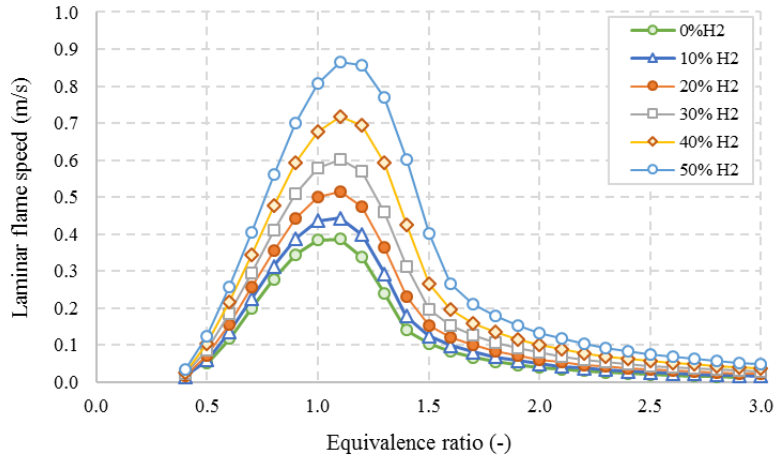

***Figure 1.5**: Laminar flame speed of methane-hydrogen air flames, at ambient temperature and atmospheric pressure*

All studies converge on a common conclusion that, laminar flame speed influences the flame position by changing its spatial location and the flame attachment points. Furthermore, presumably an increase in flame speed should decrease flame lengths. Therefore, laminar flame speed can be used to provide directional indications on fuel composition related effects.

1.2 Research object

In this context, the present work would be an attempt to address observed behavior during an experimental test campaign, improving the predictive capacity and accuracy of CFD analysis of fuel composition effects, since the preliminary design phase of combustion system.

As a matter of fact, widely used combustion models for industrial applications take advantage of a tabulated chemistry to meet both time-efficiency and fidelity. Nevertheless, such models do not properly consider the local quenching due to the elevated stretch rate at which the flame front is subjected and that directly impacts the turbulent flame speed.

In this regard, several studies show that fuel composition strongly affects the local laminar flame speed and the resistance to strain rate [5] [6], leading to non-linear behaviors of the turbulent flame. Over some particular flame stabilization regime, especially for low pilot jet penetration, a lifted flame starts stabilizing and even small C_2+ content may importantly affect lift-off height [8], since such a flame is more resistant to high strain level with respect to pure methane, impacting substantially NO_X emissions. Moreover, the effect of flame strain is particularly sensible to the local heat loss, which should be also taken into account.

When dealing with models based on flamelet assumption, such as the Flamelet Generated Manifold, one way to include the effect of strain and heat loss is the modification of the progress variable closure as prescribed by the Extended Turbulent Flame Closure model. In particular, the unstrained laminar flame speed used to calculate the turbulent velocity in the Zimont TFC model can be replaced by the laminar consumption speed

computing asymmetric counterflow strained premixed flamelets, following the approach early proposed by Tay-Wo-Chong et al. [19].
Generalizing the approach there proposed, for a given operating condition and gas composition, the effect of the strain rate and heat loss on the consumption speed is pre-tabulated within the flammability limit and used as input to the combustion model via look-up table. This work represents the first application to real gas turbine flames and fuel blends. A Scale Resolving CFD analysis of an annular combustor sector for industrial gas turbine at relevant pressure and temperature conditions for pure methane and CH_4/C_2H_6 fuel mixture was performed, showing promising results compared against available experimental data in terms of NO_X emissions and LBO prediction. Moreover, the same numerical approach was applied to a CH_4/H_2 mixture for NO_X emission calculation, with exploratory purpose.

1.3 Thesis outline

The present thesis will be organized as follows.

- *Chapter 2* in the first part reports a brief description of the experimental test rigs used during the development phase of the annular combustor for NovaLT16 gas turbine and the adopted measures. In the second part shows the experimental data demonstrating the natural gas composition effects, mainly C_2H_6 impact, on NO_X emissions and LBO margin. Also, some data points for a CH_4/H_2 fuel mixture are presented.

- *Chapter 3* is aimed at describing the numerical methodology implemented to obtain the results and outcomes of this work. The combustion modeling approach used in the LES framework is described: the effects of strain and heat loss have been included in the Flamelet Generated Manifold combustion model with the aim to consider the flame resistance to strain varying with fuel composition.

- *Chapter 4* includes the numerical analysis performed on the industrial combustor chamber implementing such approach presented in Chapter 2, comparing the results with a standard model, unstrained and adiabatic. The capability of the model to predict NO_X emissions for several operating points will be shown for three different fuel gas composition.

- *Chapter 5* illustrates the accuracy of the identified model in the prediction of lean blow-out limit for two different fuel mixtures, comparing the results against available experimental data.

- *Chapter 6* displays a summary of the main achievements of this research together with conclusions.

2 Effect of natural gas composition on combustor performance

Results of test campaigns, at relevant pressure and temperature typical of gas turbines, show the impact of natural gas composition on combustion performance [8]. An experimental characterization in terms of emissions, blowout and combustion dynamics has been carried out during the design phase of the annular combustor for a 16.5MW heavy-duty gas turbine at Baker Hughes [20].

2.1 Test rigs facilities

Two different test facilities were used during the development of the combustion system. A Full-scale Annular combustor Rig (FAR), installed in SestaLab test cell (Radicondoli, Italy) was used to characterize the combustion system operability [21]. The test cell allows to replicate different operative conditions of the gas turbine by varying independently combustion air flow, temperature (TCD), pressure (PCD) and fuel flow. A guide vane ring reproducing engine first stage nozzle flow function was put at combustor exit to obtain equivalent acoustic boundary. The test campaign was structured into a sequence of steady-state test points, representing the different operating conditions and combustion modes. A schematic description of the experimental test cell and of the test article are shown in *Figure 2.1*.

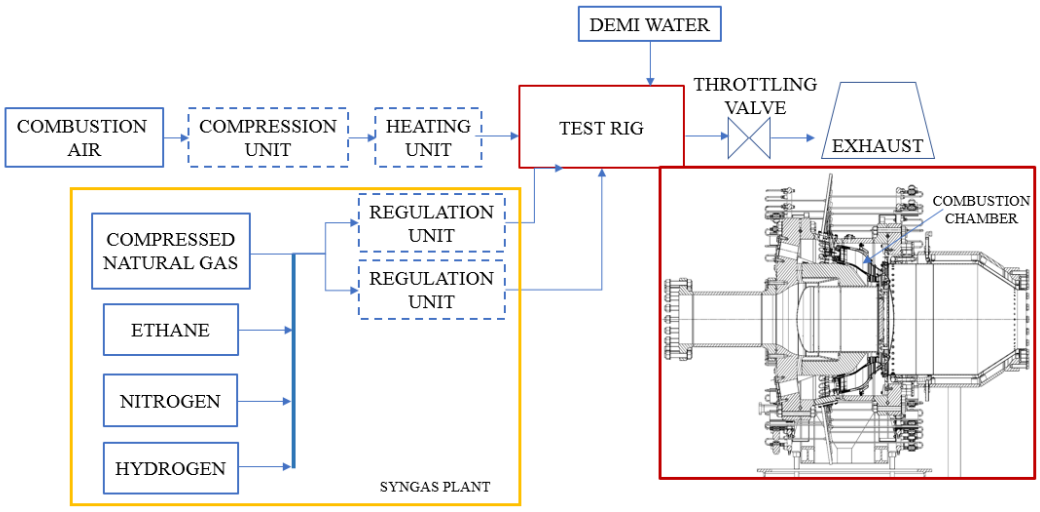

***Figure 2.1**: SestaLab test cell main features*

The combustor test cell is equipped with two sets of instruments:

- those generally called "standard", necessary for the proper control of the combustion system and the whole facilities' devices, and including fuel and air mass flows, pressure, temperatures and fuel gas composition;
- "special" instrumentation, strictly related to the combustion system for the execution of the specific test campaign and devoted mainly to monitoring; such additional instrumentation consists of static and dynamic pressure probes, and thermocouples to measure metal and gas temperatures.

For the investigation of the operative conditions and fuel composition effects on the flame shape and position and in turn on hardware durability, the combustor liners have been instrumented with several thermocouples, giving a discrete map of the metal temperature profile.

Combustion dynamics were measured by means of piezoelectric pressure probes, located in different zones of the hardware.

Exhaust-gas emissions were continuously measured and recorded during the test at different flame temperatures, pilot splits, combustor pressure drops, inlet temperatures and pressures, looking for thermoacoustic instabilities onset and lean blow-out. Two

independent emission analyzers sampling the fuel gas in two different points were used: 1) rakes located at combustion chamber exit, 2) exhaust duct. Chemiluminescence analyzers for NO_X concentration, non-dispersive infrared analyzers for CO, paramagnetic O_2 analyzers and UHC analyzers have been used.

Compressed natural gas is split and controlled into two lines (premix and pilot) required by the combustion system.

Typical measurements ranges and uncertainties are indicated in *Table 2.1*.

MEASUREMENT CHAIN	TYPICAL RANGE	UNCERTAINTY (2s)
Temperatures	(K-type) 300-800°C (B-type) 800-1500 °C	(K) 5°C @ 800°C (B) 7°C @ 1500°C
Pressures	(Gauge) 0-35 barg (Differential) 0-2000 mbar	0.8% FS
Dynamic pressure	0.5bar / 3kHz	5% - 10% (temperature dependent)
Mass flow rate	Air: 2-37 kg/s Fuel: 0.02-1 kg/s	1% FS
Fuel gas composition: CH_4, C_2H_6, C_3H_8, N_2, H_2	0 – 100%vol.	+/- 1%
Exhaust Emissions: NOx CO O_2 CO_2	0 - 25 ppm 0 - 10ppm 0 - 20%vol 0 - 5%vol	0.3 ppm (@ 25 ppm) 0.3 ppm (@ 10ppm) 0.7%vol (@ 12%vol) 0.3%vol (@ 5%vol)

Table 2.1: *Typical ranges and uncertainties of FAR measurement groups acquired*

SestaLab offers the possibility to create the desired fuel gas mixture within the context of the specific combustion test. The “Syngas Plant” is a dedicated system made mainly by

a mixing pipe into which different gas lines converge; each line contains the constituent of the gas mixture according to the desired specifications in terms of purity (e.g. CH_4 can be commercial Natural Gas or 99% pure CH_4). Appropriate gas conditions in terms of pressure, temperature and mass flow are realized in each line according to the mixing operability requirements. Then, the final fuel gas mixture is admitted to the combustor through the regulation valve, heating unit and measurements of composition and mass flow.

Figure 2.2 is a schematic representation of the "Syngas Plant" configured for the test campaign recalled in this work: ethane and hydrogen were added to natural gas at different concentrations. C_2H_6 and H_2 concentration measurement has been performed by means of an on-line gas-chromatographic analysis for monitoring purpose only.

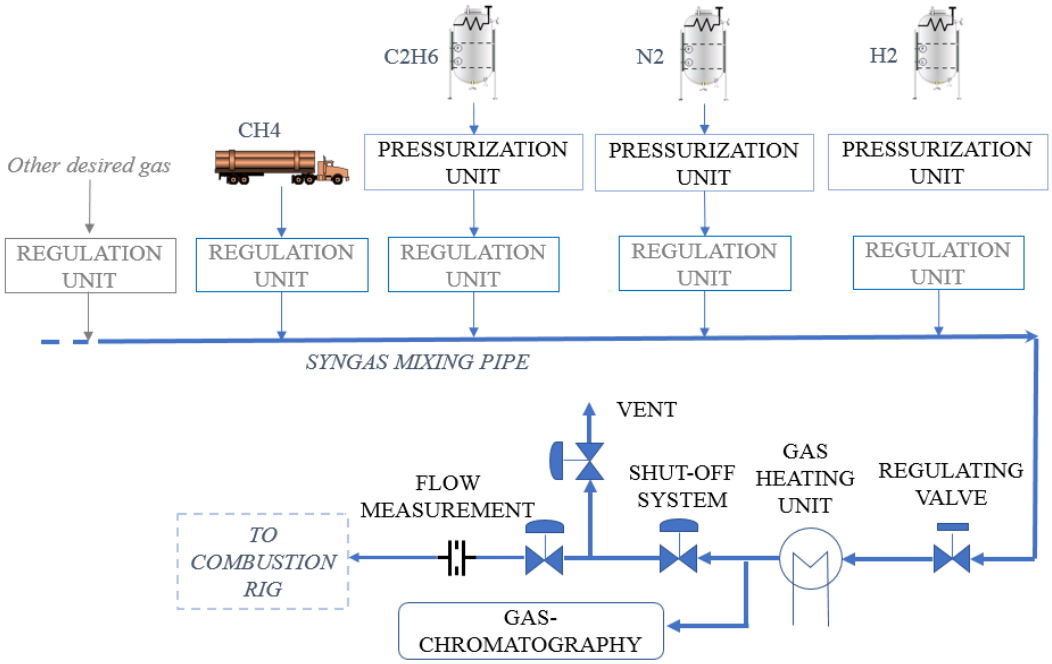

***Figure 2.2**: SestaLab Syngas Plant*

A second test rig, a prototypal engine rig (*Figure 2.3*), housed in Nuovo Pignone Tecnologie facility (Florence, Italy), was then used for validation purposes. The gas turbine

NovaLT16™ (gas generator + power turbine) has been validated in terms of performances and emissions; the gas turbine is fully packaged and connected to a power generator to vary the load from 0 to 100%, furthermore, for every load condition it has been identified the operability map of the combustor. The following groups of measurements were acquired: inlet fluids conditions (temperature, pressure and mass flow) and outlet exhaust gases conditions including the emissions (NO_X, CO, O_2) to verify the overall balances, building the combustor map and to validate the emission models. Emissions are measured in the exhaust duct with redundancy (one sampling upstream and the other downstream the silencer). An on-line gas-chromatograph allows to monitor and record the natural gas composition coming from the Italian supply network.

***Figure 2.3**: NovaLT16™ Test bench*

The combustion system features a Double Axial Counter Rotating Swirler (DACRS), whose progressive development is reported in [20] [22], as it is a widely used technology on Dry Low NO_X combustion system across General Electric. The burners have the

function to provide to the combustion zone a fuel/air mixture with adequate concentration and velocity profile, able to develop a stable flame.

The premixer, shown in *Figure 2.4*, consists of a dual passage swirler followed by a converging duct and it is featured by a transverse jet premix injection and by a coaxial pilot on nozzle tip with different injection holes angles.

Such a design promotes high turbulence levels allowing an intense mixing inside the premixer. The lean premixed flame is surrounded by discrete pilot injection points which help to stabilize the flame and are the main responsible for NO formation [23] [24].

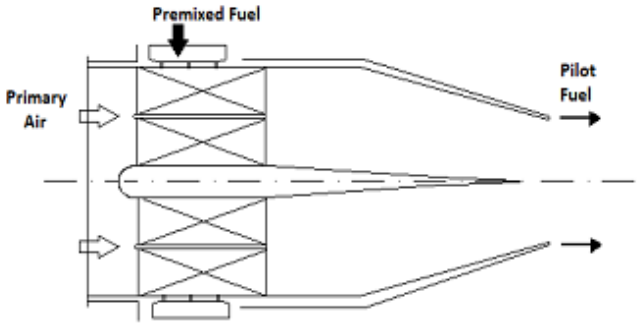

***Figure 2.4**: DACRS fuel burner scheme*

2.2 Experimental data

2.2.1 Natural gas blended with ethane

Figure 2.5 shows the map of all the explored operating conditions in terms of combustor operating temperature and fuel pilot split at different gas C_2H_6 content during the full engine test campaign. Operating temperature (Ta) is normalized with respect to the design reference value (Ta_0) as well as pilot split (Ps) is normalized with respect to the lowest pilot reached with pure methane (Ps_0).

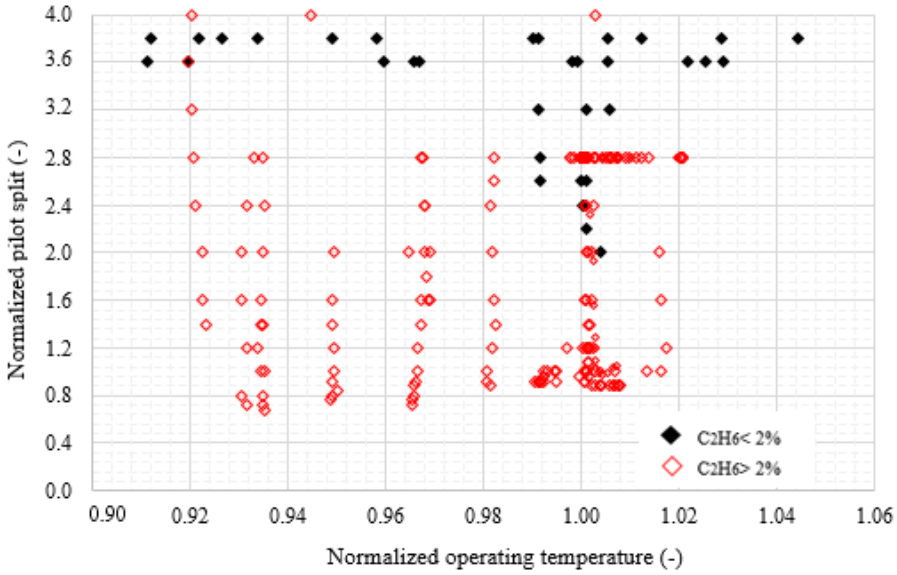

***Figure 2.5**: Map of explored points*

The composition effect is already clear, only mixture blended with ethane, even in small percentage, are able to operate with lower temperature and fuel pilot split.

In *Figure 2.6* and *Figure 2.7*, for a sub-set of data, the NO_X emissions and the pressure pulsations root mean square measured during the tests are plotted as a function of normalized pilot fuel split for 100%CH_4 and 85%CH_4-15%C_2H_6 fuel mixture at ISO-base load condition and operating temperature Ta0.

The emissions data set, as well as the pressure pulsations, is normalized against the value at the lowest pilot split and pure methane.

Working with 100%CH_4 mixture at combustor operating temperature Ta0, the combustion system is able to achieve the lowest emissions level for pilot split equal to 1.0. The limit to the further reduction of NO_X emissions is represented by LBO occurrence clearly identified by combustion dynamics onset.

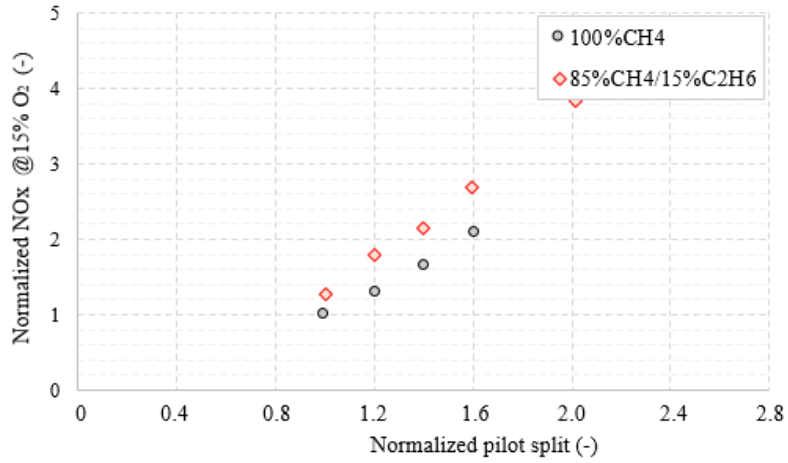

***Figure 2.6**: Normalized NO_X emissions at ISO-base load condition*

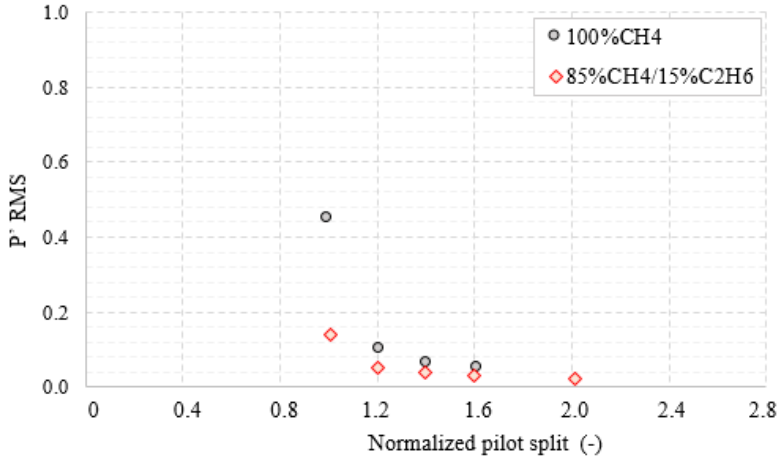

***Figure 2.7**: Normalized pressure pulsation RMS at ISO-base load condition*

Moreover, decreasing the operating temperature, higher pilot fuel flow rate must be kept to ensure flame stability and so not resulting in lower emissions.

CH_4-C_2H_6 fuel blend leads to NO_X emissions increase with same pilot fuel split with respect to a mixture of pure methane.

Nevertheless, even for modest amount of ethane, the increase of blowout margin allows to operate with lower operating temperature and pilot split resulting in a global reduction of NO_X emissions while keeping pressure pulsations below threshold as well as sufficient margin to blow-out. This behavior was verified during a FAR test campaign assessing the sensitivity to operating temperature for a 85%CH_4-15%C_2H_6 mixture as shown in *Figure 2.8*.

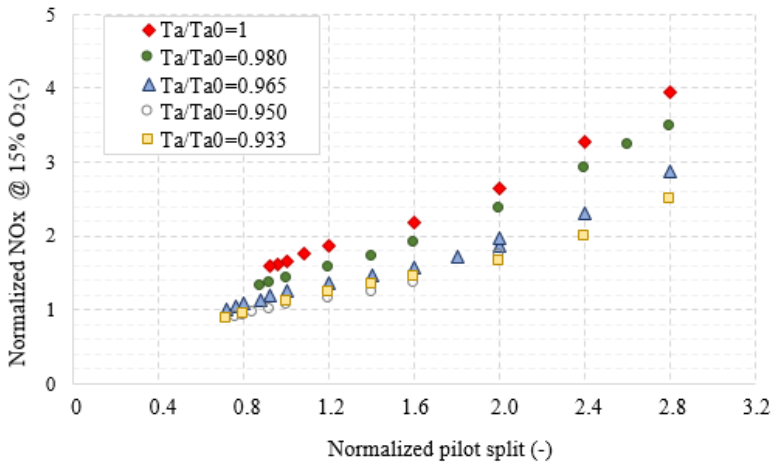

***Figure 2.8**: Normalized NO_X emissions at ISO-base load conditions for different operating temperatures and for 85%CH_4-15%C_2H_6 fuel mixture*

Therefore, gas C_2H_6 content leads to substantially enlarge LBO margin keeping down the thermoacoustic instabilities. On the other hand, to meet NO_X emission level, lower operating temperature with respect to design one was needed.

Figure 2.9 shows how much the operating temperature shall be decreased from its design value to keep NO_X below target at different ethane content in the fuel gas mixture. Trend line is obtained as a linear regression of the available experimental data.

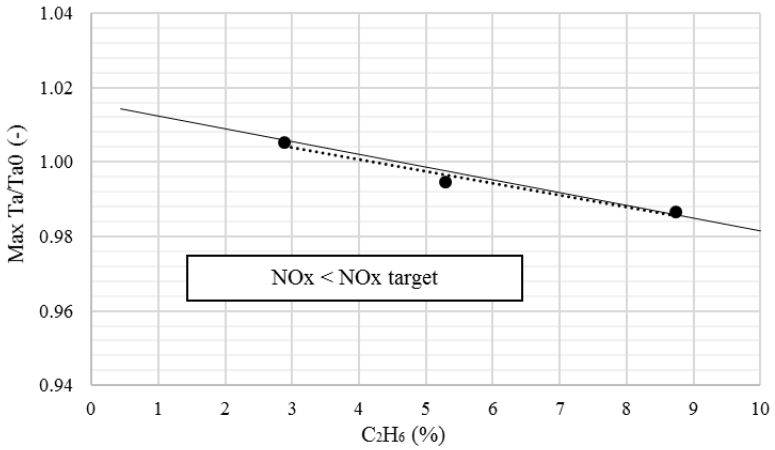

***Figure 2.9**: Maximum operating temperature for varying C_2H_6 content*

Experimental data gathered during full annular combustor rig and engine test campaign allowed to define the limits of the burner operability region in terms of operating temperature and pilot split, imposed by LBO occurrence, combustion dynamics onset and NO_X emissions target level.

Figure 2.10 shows the resulting operating areas identified. Blue and yellow triangles represent respectively the safe operating area for a fuel composition 100%CH_4 and 85%CH_4-15%C_2H_6.

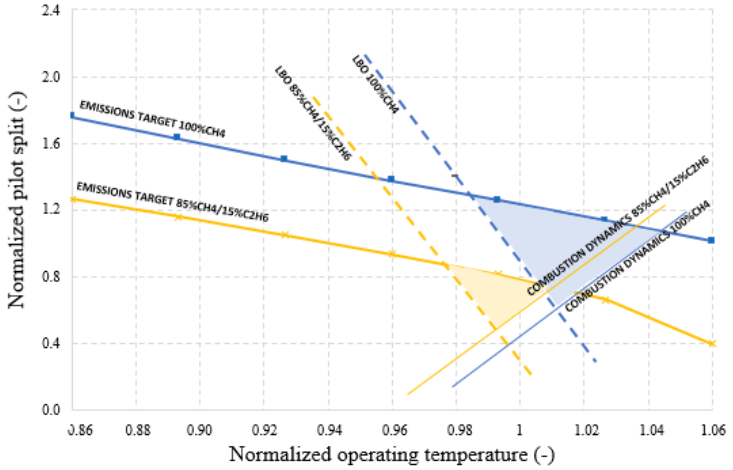

***Figure 2.10**: Viable operating areas at ISO-base load condition*

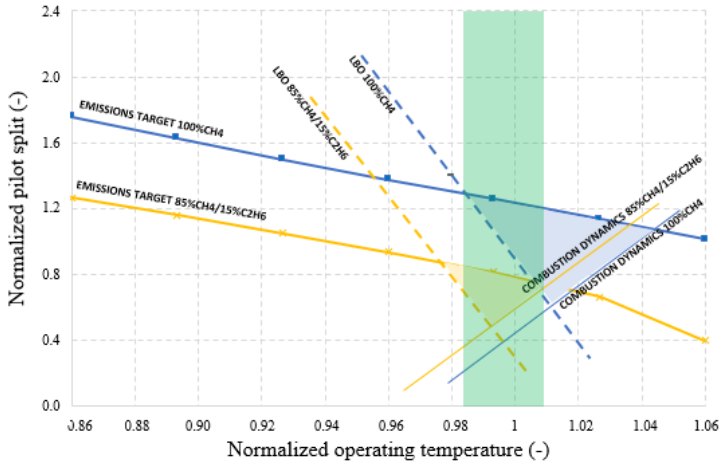

***Figure 2.11**: Viable operating temperature window at ISO-base load condition*

CH_4-C_2H_6 fuel blend increases blowout margin allowing to operate with lower operating temperature and pilot split and reaching a global reduction of NO_X emissions.

A viable operating point for the combustion system, for typical natural gas composition, can be identified in the temperature window delimitated by the green region reported in *Figure 2.11*. The requirement to operate at different pilot split in function of gas composition is fulfilled by an active combustion control system, based on closed loop algorithms, that by means of an indirect evaluation of gas composition adjust the operating point to achieve optimum combustor performance, minimizing pollutant emissions at all operating conditions.

2.2.2 Natural gas blended with hydrogen

In the framework of the same test campaign, also the influence on NO_X emissions of H_2 blended natural gas up to 30% have been investigated on a limited set of data points. The different thermodynamic properties of H_2 affect the flow field above the burner in many ways (calorific value, density, differential diffusion) requiring flow field analysis to ensure that the burner can operate with H_2 and maintain high combustion efficiency and low

pollutant emissions on a stable operating condition. Test was conducted at the same pressure and temperature of the previous ones and keeping constant the thermal power.

By comparison with the baseline natural gas composition, the NO_X emissions appear to increase exponentially with H_2 addition, with almost 150% increase in the baseline NO_X level at 30% H_2, *Figure 2.12*. This is can be attributed to locally high flame temperatures and non-perfect mixing.

Moreover, studies show that the LBO limit can be extended by 9-10% in terms of equivalence ratio with 20%vol H_2 addition compared with a pure CH_4 flame [25] [26]. The consequence of this lean operability shift is a corresponding reduction in NO_X emissions due to reduced firing temperatures, with a maximum reduction of 35% compared to pure CH_4 flames.

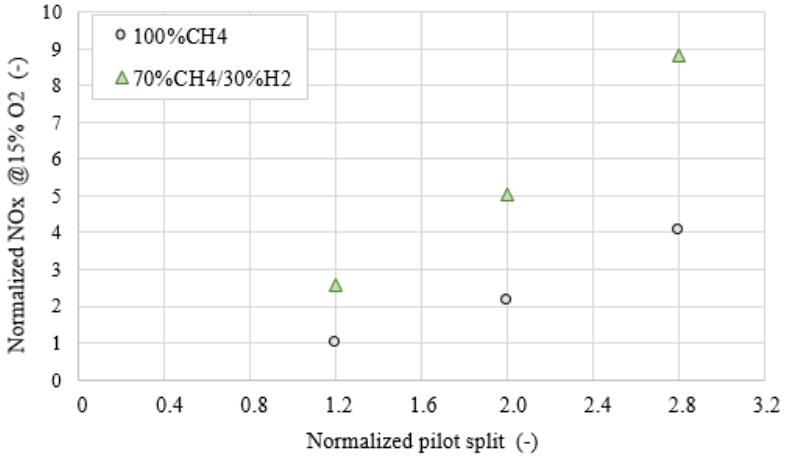

***Figure 2.12**: Normalized NO_X emissions at ISO-base load condition for CH_4-H_2 blend*

To address the observed phenomena and to take into account the effect of the fuel composition since the beginning of the design process of a combustion system, it becomes necessary to investigate and identify the main parameters, related to the fuel composition, having effect on GT combustion operation and emissions and transfer them to a predictive CFD model. Experimental investigations on combustors are technically demanding and economically expensive. Furthermore, many areo-engines and industrial turbines employ annular combustors and these cannot be reproducing by a sector, not allowing to save, in

addition, the design and operation of reactive test rig present several challenges. For these reasons, the development and validation of accurate CFD tools is fundamental as to get a better and wider understanding of the physics involved in the interaction between fuel composition variation and combustion mechanisms.

3 Numerical modeling of fuel composition effect

Nowadays, CFD has an essential role in the industrial environmental and research community. The use of advanced numerical tools during the design phase represents one of the main drivers for the development of turbomachinery components, leads to results in a rapid and economical way, if compared with prototyping and experimentation. Nevertheless, the application of classical numerical techniques to the combustion presents some aspects requiring further investigation. This dissertation is focused on modeling improvement of fuel composition effect.

3.1 Numerical methods

Most of technically relevant fluid flows are turbulent as well as the flow field within a gas turbine combustion chamber. Turbulence consists of a field of nested eddies of decreasing size where the kinetic energy of the turbulence is transported, with negligible dissipation, from the largest eddies (energy containing eddies) to those gradually smaller up to the Kolmogorov scale , where the viscosity, which is no longer negligible, attenuates turbulent fluctuations, *Figure 3.1*. The large eddies interact with the mean flow and extract energy from it.

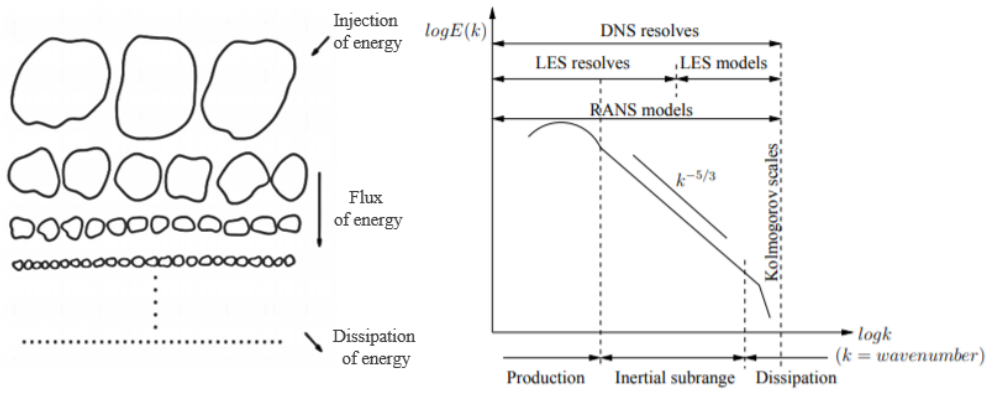

***Figure 3.1**: Resolved and/or modeled turbulence scales by DNS, LES, RANS [27]*

In order to simulate turbulent flows, three different approaches are used for resolution of Navier-Stokes (NS) equations:

- Direct Numerical Simulation (DNS) consists in the pure solution of the three–dimensional, instantaneous Navier– Stokes equations, no turbulence model or empirical closure assumptions are required. It can be considered as the most accurate method for the simulations of turbulent flows. However, the computational effort for DNS is very high even at a moderately high Reynolds number, the computational cost scales up with Re^3 [28]. In DNS, the main effort is devoted to the dissipation range (see *Figure 3.1- right*) and this effort increases with the Reynolds number [29].
- Large Eddy Simulation (LES) is aimed at resolving only larger eddies, while the smaller scales are treated by sub-grid scale models (SGS). In other words, the large scales, that are responsible for most of the momentum and energy transport directly, are solved as in DNS, the smaller scales, that have a much more homogeneous and isotropic structure, are treated by SGS models. As such, LES is computationally more efficient than DNS and may be also relatively accurate. These features make the use of LES approach very attractive especially for the detailed analysis, consequently it is used in the present work.
- Reynolds Averaged Navier-Stokes (RANS) technique is based on a statistical description of turbulent flows, with the whole spectrum of turbulence length scales

being modeled. The RANS approach therefore greatly reduces the required computational effort and resources and is widely adopted for practical engineering application.

3.2 Large Eddy Simulation

Large eddy simulation approach computes the largest structures of the flow field (typically structures larger than the computational mesh size) whereas the effects of the more isotropic small scales are modeled. The transition between resolved and modelled scales is obtained by the filtering operation of the NS equation, which is in most cases linked to the mesh size.

According to the Pope's criterion (Eq. (3.1)) the grid must be sufficiently finer as to enable the direct resolution (k_{res}) rather than the modelling (k_{mod}) of at least 80% of the turbulent kinetic energy.

$$M_P = \frac{k_{res}}{k_{res} + k_{mod}} \geq 0.8 \tag{3.1}$$

Applying the filtering process on the instantaneous equations leads to the filtered equations of conservation of mass and momentum of the flow, for which the turbulent subgrid scale stress is to be modelled for closure purposes.

Several modeling approaches for the small scales have been developed. The first subgrid–scale model based on an eddy–viscosity concept is proposed by Smagorinsky [30], it describes the proportionality between the subgrid scales and the large scale strain rate tensor and the characteristic subgrid mixing length can be evaluated by the Smagorinsky constant and the filter width. The value of the eddy viscosity can vary both in space and time depending on the structure of turbulence. In the present work, the subgrid eddy viscosity is modeled using the Dynamic Smagorinsky-Lilly model [31], the difference is

that the Smagorinsky constant is replaced by a parameter, which evolves dynamically in space and time.

3.2.1 Combustion modelling

The characteristic length and time scales where combustion takes place are typically well below the resolved grid scales, and the combustion process has to be modeled entirely at the subgrid level. However, the full description of chemical reactions in flames may involve hundreds of species and thousands of reactions. Handling such complex chemical schemes in turbulent combustion could be impossible for three main reasons:

- One additional balance equation is required for each species.
- Chemical reaction rates and transport coefficients are complex functions of species mass fractions and temperature; increasing the number of chemical reactions dramatically increases the computational time.
- A major difficulty is the coupling between turbulence and combustion. As chemical reactions involve a large range of chemical time scales, this coupling cannot be handled through a single turbulent time.

For this purpose, many numerical models have been developed in order to reduce the costs of flame simulations for engineering applications. Among several numerical combustion models proposed for gas turbine combustion flows, the The Flamelet-Generated Manifold (FGM) method has attracted great attention [32], for both premixed and non-premixed turbulent combustion and it was also used in this work to model the turbulent combustion. The use of FGM as a combustion model shows that combustion features at gas turbine conditions can be satisfactorily reproduced with a reasonable computational effort. The FGM method assumes that a turbulent flame can be seen as an ensemble of thin, laminar, locally one-dimensional flames, called *flamelets*, embedded within the turbulent flow field.

Laminar flamelet methods [33] are based on the idea that flame structures are much thinner than most scales of the distortions in the flow, also implying that the chemical reactions are very fast compared to all other time scales.

In the FGM technique the dynamics of the reaction is parameterized in terms of mixture fraction *z* and progress variable *c* (defined as a normalized mass fraction of products such that c = 0 in the unburnt mixture and c = 1 in the products), for which transport equations are solved during run-time. And here lies one of the main strengths of the FGM method: the number of independent control variables can be increased for a better description of the combustion phenomena.

The implementation of FGM method consist of computing flamelet system in a pre-processing phase with a proper 1D flame code, coupled with a suitable chemical reaction mechanism and under the appropriate condition representative for the combustion system to which the model will be applied. The generated flamelets are stored in a tabulated form and during the CFD run, the code retrieves thermochemical variables from the table for given values of the control variables.

In the present work, The Ansys Fluent® built-in solver was exploited to tabulate chemistry by 1D laminar diffusion flamelets using the detailed reaction mechanism GRImech 3.0 [34]. The laminar results were then pre-integrated with presumed β-shaped probability density functions to account for turbulent fluctuations and stored as manifold.

In the simulation initialization phase, the database is loaded into memory, then the CFD code must solve transport equations for the control variables, together with the momentum and continuity equations. The transport equations for the control variables *c* and *z* are expressed using the Favre-averaged filtering, as for Fluent solution process:

$$\frac{\partial \bar{\rho}\tilde{z}}{\partial t} + \frac{\partial \bar{\rho}\widetilde{u_i}\tilde{z}}{\partial x_i} = \frac{\partial}{\partial x_i}\left(\bar{\rho} D_{tot} \frac{\partial \tilde{z}}{\partial x_i}\right) \tag{3.2}$$

$$\frac{\partial \bar{\rho}\tilde{c}}{\partial t} + \frac{\partial \bar{\rho}\widetilde{u_i}\tilde{c}}{\partial x_i} = \frac{\partial}{\partial x_i}\left(\bar{\rho} D_{tot} \frac{\partial \tilde{c}}{\partial x_i}\right) + \overline{\dot{\omega}_c} \tag{3.3}$$

Where $\bar{\rho}$ is the Reynolds averaged density, $\widetilde{u_i}$ is the i-component of velocity and $\overline{\dot{\omega}_c}$ is a source term of the progress variable. The closure is obtained by making the usual gradient diffusion assumption, where the eddy diffusivity is obtained from the turbulent viscosity ν_t by assuming of the existence of a turbulent Schmidt number [35]:

$$D_{tot} = D + D_t = \frac{\nu}{Sc} + \frac{\nu_t}{Sc_t} \tag{3.4}$$

The source term for the progress variable is modeled by:

$$\overline{\dot{\omega}_c} = \rho_u S_t |\nabla \tilde{c}| \tag{3.5}$$

Where ρ_u is the density of unburnt mixture and S_t is a turbulent flame speed that depends on the physico-chemical characteristics of the combustible mixture and the local turbulence at the subgrid level.

3.2.2 Zimont's model of the turbulent flame speed

For a complete closure, a model for the turbulent flame speed S_t is needed. Zimont proposed a model, Turbulent Flame speed Closure model (TFC) [36], for S_t which is valid in the "thickened-wrinkled" flame front (*Figure 3.2*). The model is strictly applicable when the smallest turbulent eddies in the flow (the Kolmogorov scales) are smaller than the flame thickness and penetrate into the flame zone. This regime is characterized by very large Reynolds numbers and moderately large Damkohler numbers not enough for the combustion to occur in the laminar flamelet regime ($Re \gg 1$, 1< Da < $Re^{1/2}$).
Zimont's analysis for this regime led to the following expression for the turbulent flame speed:

$$\frac{S_t}{S_l^0} \simeq (Re\ Pr)^{1/2} Da^{-1/4} \tag{3.6}$$

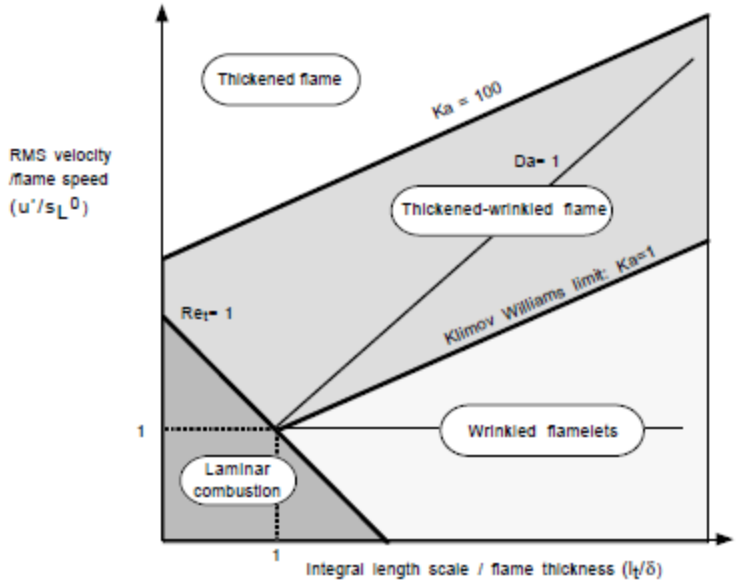

***Figure 3.2**: Turbulent combustion diagram [37]*

expressed via the Reynolds, Damkohler and Prandtl numbers:

$$Re = \frac{u' L_t}{\nu}\,, \quad Da = \frac{\tau_t}{\tau_c}\,, \quad Pr = \frac{\nu}{\alpha} \tag{3.7}$$

u', L_t and τ_t are the integral scale of turbulence; ν and α are the kinematic and thermal diffusivity; $\tau_c = \frac{\delta_l^0}{S_l^0}$ is a characteristic chemical time scale; δ_l^0 and S_l^0 are the unstretched thickness and lamina flame speed, which is, in turn, determined by the fuel concentration, temperature, and molecular diffusion properties, as well as the detailed chemical kinetics. Combining the expressions (3.7) in the Eq. (3.6), the final formulation results:

$$S_t = A\ u'^{\frac{3}{4}}\ S_l^{0\frac{1}{2}}\ \alpha^{-\frac{1}{4}}\ L_t^{\frac{1}{4}} \tag{3.8}$$

All parameters appearing in the Eq. (3.8) are either constants describing physico-chemical properties of the combustible mixture or derived turbulence model, it does not contain empirical information except for the constant A (which should be of order unity). Changes in simulated operating condition (pressure, temperature) and fuel composition will affect parameters α and S_l^0 and thereby influence the value of S_t, in a physically meaningful way.

3.2.3 Flame stretch effect

Eq. (3.8) leads to larger flame speeds for increasing turbulence intensity; Instead, at very high levels of turbulence intensity, it is observed experimentally that the turbulent burning rate is limited or may even decrease [38]. This because the stretch effect is not taken into account. A flame front propagating in a non-uniform flow is subject to strain and curvature effects which lead to changes in flame area: these changes are measured by stretch [37]. This "stretch effect" is of importance for low emission gas turbines and have to be incorporated in any combustion model, in particular if flame stability phenomena have to be analyzed, flame stretching will have a significant effect reducing the local flamelets velocities and even cause their extinction.

This effect has been incorporated in Eq. (3.8) by introducing a stretch parameter G as a correction factor for the turbulent burning velocity [38], which we adopt here at the velocity subgrid level. This stretch factor represents the probability that the stretching will not quench the flame; if there is no stretching (G=1), the probability that the flame will be unquenched is 100%:

$$G = \frac{1}{2} erfc\left\{-\sqrt{\frac{1}{2\sigma}}\left(ln\left(\frac{\varepsilon_{cr}}{\varepsilon}\right) + \frac{\sigma_\varepsilon}{2}\right)\right\} \tag{3.9}$$

$$\varepsilon_{cr} = 15\nu g_{cr}^2 \quad \sigma_\varepsilon = \mu_{str} ln\left(\frac{L_t}{L_k}\right) \tag{3.10}$$

Where σ_ε is the standard deviation of the ε distribution, μ_{str} is a constant of value 0.26, ε_{cr} is the turbulence dissipation rate at critical strain g_{cr}.
Differently strained flamelets are reduced to unstrained ones (no quenching) if the absolute value g of the velocity gradient is less than some critical value g_{cr}, or to highly strained flamelets for $g > g_{cr}$. The g_{cr} value should be adjusted based on experimental data for the burner, nevertheless, a reasonable model for the critical rate of strain is:

$$g_{cr} = \frac{B\, S_l^{0\,2}}{\alpha} \tag{3.11}$$

where B is a constant around 0.5.

3.3 Combustion modelling including stretch and heat loss effects

The FGM turbulent combustion model take into account the effect of the strain by considering a corresponding critical strain rate, as discussed in the previous section. Despite the success of this model, considering a unique constant g_{cr} it is not very accurate to describe the stretch effect on turbulent flame speed.

Stretching a flame means feeding it with more fresh gases (because fuel mass fraction gradients are increased), but also includes cooling the flame front more intensely (because the temperature gradients are increased). This effect is strongly dependent on preferential diffusion, where differences in the relative rates of mass diffusion and thermal diffusion, usually expressed in term of Lewis number, affect the tendency of the flame to become wrinkled. This effect is particularly important in case of fuel composition variation; indeed,

this strongly affects the local laminar flame speed and the resistance to strain rate [5], leading to non-linear behaviors of the turbulent flame. Moreover, a second parameter controlling the flame response is the level of heat losses, which should be also taken into account.

A possible consequence of ignoring a reliable modeling of stretch and the effects of heat losses are the incorrect predictions of the flame shape, heat release distribution [19], and no capturing of fuel composition effects. This may lead to inadequate predictions of flame stabilization regions and hence NO_X emissions, flame dynamics and thermal load over the combustor.

Studies show that, the response of the flame to stretch, consisting of strain and curvature, and heat losses can be analyzed by the effects on the laminar flame speed, which is an important parameter to describe the behavior of a flame.

In a laminar flame, three different speed can be identified: absolute speed S_a , displacement speed S_d and consumption speed S_c. An important difference is that S_a and S_d are local quantities while S_c is a quantity resulting from an integral of the reaction rate across the flame front. It is more meaningful to focus on the consumption speed S_c which is unambiguously defined. It measures the speed at which the flame burns the reactants [39]:

$$S_c = -\frac{1}{\rho_u Y_F} \int_{-\infty}^{+\infty} \dot{\omega}_F \, dn \tag{3.12}$$

where ρ_u is the unburned gas density, Y_F the mass fraction of fuel and $\dot{\omega}_F$ the mass burning rate of fuel per unit volume.

Through several theoretical and experimental studies over the past decades, it has been established that the flame speed is linearly proportional to stretch κ in the weak stretch limit:

$$\frac{S_c}{S_l^0} = 1 - Ma\, Ka \tag{3.13}$$

Where Ka is the Karlovitz number representing stretch and the proportionality constant Ma is the Markstein number. Asymptotic analysis showed that the Markstein number is a function of thermodynamic and transport properties of the mixture [40], such that it can assume positive or negative values depending on the diffusivity of the reactant species:

$$Ka = \frac{\delta_u}{S_l^0}\kappa \qquad Ma = \frac{\mathcal{L}}{\delta_u} \tag{3.14}$$

Where $\mathcal{L}$ in the Markstein length and $\delta_u$is the laminar flame front thickness.

Besides strain, heat losses have also to be taken into consideration because its effect decrease the flame temperature and the chemical reaction rates. Sun and Law [41] derived a non-linear relation for the flame thickness under the influence of strain and heat losses:

$$\frac{\delta_u}{\delta_u^0} \sim e^{-\theta} \tag{3.15}$$

with

$$\theta = \frac{Ze}{2}\left(1 - \frac{T_f - T_u}{T_{ad} - T_u}\right) \qquad Ze = \frac{E_a}{RT_{ad}^2}(T_{ad} - T_u) \tag{3.16}$$

Where T_u is the unburnt premixture temperature, T_{ad} the products temperature at adiabatic conditions, T_f the flame temperature refers to the maximum temperature along the flame. The Zeldovich number Ze in then defined as function of activation energy E_a and universal gas constant R.

The consumption speed of a premixed flame in related to its thickness with the relation [42]:

$$\frac{S_c}{S_l^0} \sim \frac{\delta_u}{\delta_u^0} \sim e^{-\theta} \tag{3.17}$$

And this relation motivates the empirical relation formulated by Tay-Wo-Chong et al. [43] [44]:

$$S_c = S_l^0 \exp[-Ka(Ma + \varphi)] \tag{3.18}$$

Where φ is the heat loss parameter expressed by:

$$\varphi = \frac{E_a}{2RT_{ad}}\left(\frac{1-\beta}{\beta^4}\right) \tag{3.19}$$

with the normalized heat loss coefficient β defined by:

$$\beta = \frac{T_{prod} - T_u}{T_{ad} - T_u} \tag{3.20}$$

which takes into account the effects of variation in T_{prod} and indicates a level of adiabaticity (β=1 for adiabatic and β < 1 for non-adiabatic conditions).

To investigate strained laminar flamelets in an extended range of strain rates, counterflow configurations are commonly used in asymmetric configuration in which hot combustion products are sent against a flow of fresh gases ("fresh-to-burnt"), *Figure 3.3*.

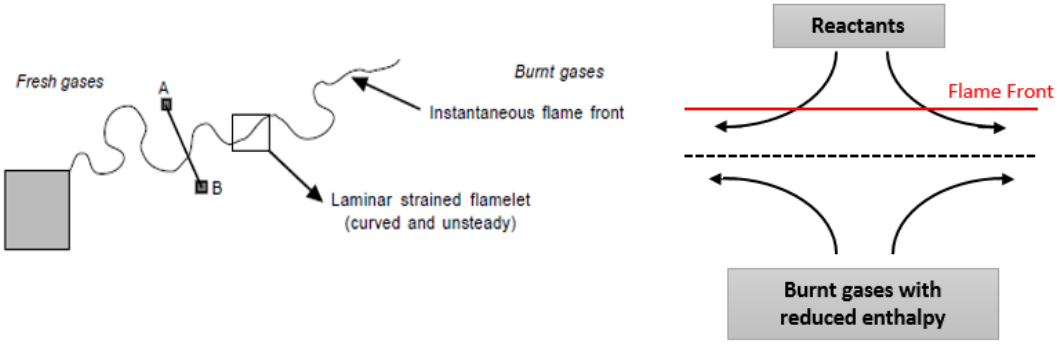

***Figure 3.3**: Flamelet surface concept for turbulent premixed flame*

In this case, the flame is stretched because the velocity in the flame tangent plane changes rapidly. The velocities in a potential flow are defined as:

$$u = -ax \tag{3.21}$$

$$v = ay \tag{3.22}$$

Where a is the strain rate defined by the velocity gradient in the unburnt side of the flame:

$$a = -\frac{du}{dx} \tag{3.23}$$

Numerical simulations of steady laminar flames in the asymmetric counterflow arrangement were carried out with the program RUN1DL by Tay-Wo-Chong et al. [19] using the detailed chemical reaction mechanism GRI-3.0. Mixtures of methane-air with equivalence ratios ϕ ranging from ϕ =0.59 to 0.83 were considered, with unburnt mixture temperature T_u = 293 K at an operating pressure of 1 atm. The consumption speed was calculated using Eq. (3.12) for different strain rates, burnt side temperature and equivalence ratios. In *Figure 3.4*, the dependence of the consumption speed for φ=0.71 on burnt side temperature and strain rate is shown as a 3D distribution (left) and a 2D representation (right).

At low strain rates the reaction zone was far to the right of the stagnation zone, there was very little diffusive transfer of heat from the reaction zone to the burnt side, such that the products generated by the flame reach temperatures close to the adiabatic flame temperature T_{ad} and the consumption speed was not significantly affected by heat losses. On the other hand, for strain rates higher than 100 1/s, the sensitivity of the consumption speed to strain is increased in the presence of heat losses: the consumption speed decreased gradually with decreasing T_{prod}.

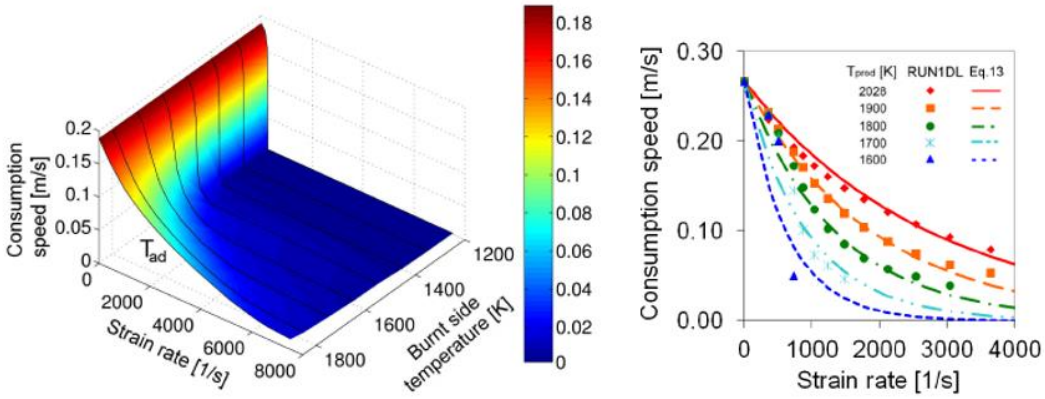

***Figure 3.4**: Consumption speed dependence on strain rate and burnt temperature for methane-air mixture [19]*

At this point, it is possible to include the effect of stretch and heat loss in the combustion model. In the TFC combustion model, the unstretched laminar flame speed can be replaced by the consumption speed depending on strain and heat loss, not considering the stretch factor *G*. The Extended Turbulent Flame Closure (ETFC), proposed by [44] and successfully applied in RANS and LES simulations of turbulent atmospheric flames [45], describe the turbulent flame speed as:

$$S_t = A\ u'^{\frac{3}{4}}\ S_c^{\frac{1}{2}}\ \alpha^{-\frac{1}{4}}\ L_t^{\frac{1}{4}} \tag{3.24}$$

In general, the consumption speed S_c depends on the fuel, the operating conditions, the flame strain rate a and the burnt gas temperature:

$$S_c = S_c(p, T_u, \phi, a, T_b) \tag{3.25}$$

Since the model requires as fundamental input the consumption speed, the above dependence must be described accurately. The semi-empirical correlation developed by Eq.(3.18) is valid for lean methane-air atmospheric flames only. Despite the correlation gives accurate results in its validity range, it is not suitable for the application in real gas

turbine combustors environment. The formulation of a more general correlation with extended applicability range is considered unpractical for industrial applications, which involve wide variation of operating parameters, since the data regression should be carried out each time. As an alternative, a discrete description of the consumption speed through a look-up table can be obtained by the numerical solution of one-dimensional laminar flames at the conditions of interest [19] [46]. Once evaluated at the desired pressure, unburnt temperature and fuel composition, the consumption speed look-up table can be accessed during the CFD simulation and used to evaluate the turbulent flame speed. However, the latter operation requires the definition of the flame strain and heat loss correction parameter ψ in the unsteady turbulent flow-field whit which read in the table the corresponding consumption speed value for each point in the flow field. The following section describes specifically these modellings in LES. The present tabulation approach, which provides high flexibility and avoids the definition of complex analytical correlations, was previously tested and validated in stratified atmospheric flame [47].
This work represents the first application to real gas turbine operating condition and fuel blends.

3.3.1 Stretch and heat loss modelling in LES

The flame stretch for a thin front can be defined as [37]:

$$\kappa = \left(\delta_{ij} - n_i n_j\right) S_{ij} + S_l \frac{\partial n_i}{\partial x_i} = a + \sigma_c \tag{3.26}$$

where the $\boldsymbol{n}$ is the flame front normal, $S_{ij} = \partial u_i / \partial x_j$ the fluid strain rate, S_l the laminar flame speed. The two terms represent respectively the strain a and the curvature σ_c. As reported in [48], in very turbulent flows ($Ka > 0.1$) the curvature contribution to stretch is much lower than the strain one. Recently, Klarmann et al. [49] evaluated both the terms in RANS framework for a methane-air burner, obtaining a one-order of magnitude difference between the terms. In the present work, the instantaneous LES flame front is expected to

present higher curvature but also strain values, leaving roughly unaltered the relative contribution. For the reasons explained above, confirmed by preliminary calculations, the curvature is neglected in the simulations, so that:

$$\kappa \simeq a \tag{3.27}$$

The stretch definition can be filtered in LES approach, separating the resolved flow-field and the sub-grid turbulence parts:

$$\tilde{a} = \left(\delta_{ij} - \widetilde{n_i n_j}\right)\frac{\partial \widetilde{u_i}}{\partial x_j} + \left[\widetilde{\left(\delta_{ij} - n_i n_j\right)\frac{\partial \mathrm{u_i}}{\partial x_j}}\right] = \tilde{a}_{res} + \tilde{a}_{sgs} \tag{3.28}$$

The resolved strain $\tilde{a}_{res}$ can be evaluated from the fluid strain rate and the resolved flame front normal vector, here described as:

$$\boldsymbol{n} = -\frac{\nabla \tilde{c}}{|\nabla \tilde{c}|} \tag{3.29}$$

The sub-grid turbulent strain requires complex specific modelling. It can be expressed in function of the sub-grid turbulent kinetic energy k_{sgs}, the filter length Δ and the efficiency function Γ_k:

$$\tilde{a}_{sgs} = \Gamma_k \cdot \frac{\sqrt{k_{sgs}}}{\Delta} \qquad with \qquad k_{sgs} = \left(\frac{\nu_{sgs}}{\Delta}\right)^2 \tag{3.30}$$

The function Γ_k accounts for the reduced ability of the small sub-grid eddies to stretch the flame front. It was introduced by [50] fitting DNS results within the Intermittent Turbulence Net Flame Stretch (ITNFS) model:

$$\log_{10}\Gamma_k = -\frac{1}{s+0.4}e^{-(s+0.4)} + \left(1-e^{-(s+0.4)}\right)(s\sigma - 0.11) \tag{3.31}$$

$$s = \log_{10}\left(\frac{\Delta}{\delta_l^0}\right), \quad \sigma = \frac{2}{3}\left(1-\frac{1}{2}\exp\left[-\left(\frac{u'_\Delta}{S_c^0}\right)^{1/3}\right]\right) \tag{3.32}$$

with δ_L^0 the laminar flame front thickness.

As far as concerns the heat loss, the parameter $\psi = T_b/T_{eq}$, which represents the departure from the adiabatic equilibrium temperature, cannot be directly evaluated since it is formally defined only in the laminar flamelet products. In the FGM framework ψ should be defined for all the progress variable values, so it was associated to the ratio of the temperature to the adiabatic local temperature:

$$\psi = \frac{T_b}{T_{eq}} \simeq \frac{T(Z, Z''^2, c, c''^2, h)}{T_{ad}(Z, Z''^2, c, c''^2, h_{ad})} \tag{3.33}$$

According to this formulation of ψ, in the burnt gas where $c = 1$ exact definition is retrieved.

Eqs. (3.28-3.32) and (3.33) are evaluated at each cell of the fluid domain to obtain the local values of flame front stretch and heat loss correction. A dedicated User-Defined Function has been implemented in Fluent for their computation during the CFD simulation.

3.4 Consumption speed tabulation

3.4.1 Method

The tabulation of the consumption speed requires a dedicated pre-processing step, where one-dimensional laminar flames are solved. In the present work, Python library Cantera v2.4.0 [51] was exploited to solve counterflow fresh-to-burnt premixed flames,

using the detailed reaction mechanism GRImech-3.0. Thousands of flames were calculated, varying independently:

- equivalence ratio Ø, between flammability limits of the considered fuel mixture;
- strain rate *a*, by increasing the axial velocity of opposed flows up to a maximum value characteristic of the analyzed flow field. Numerically it is defined as the maximum axial strain with lower axial coordinate (*Figure 3.5*):

$$a = \frac{du}{dx} \tag{3.34}$$

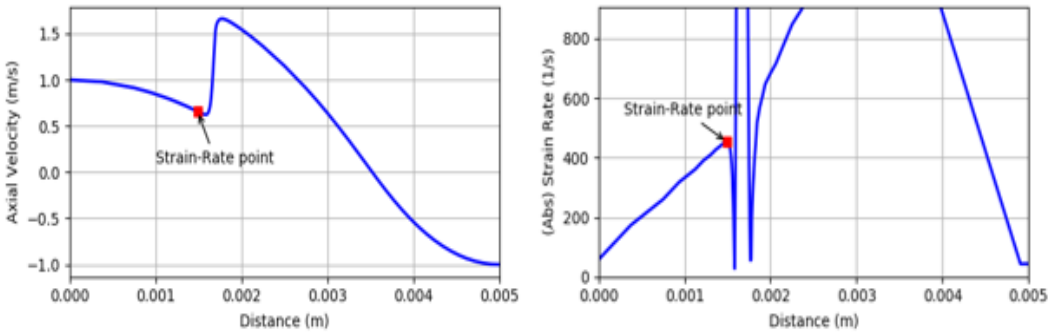

***Figure 3.5**: Axial velocity and strain profile across premixed flame front*

- burnt gas temperature ratio to adiabatic equilibrium temperature $\psi = T_b/T_{eq}$, in a proper range allowing to take into account the heat loss contribution.

Defining and estimating a flame thickness before computation is an obvious requirement because this thickness controls the required mesh resolution along the distance between the two jects: the flame structure must be resolved, and enough points must be localized within the flame thickness.

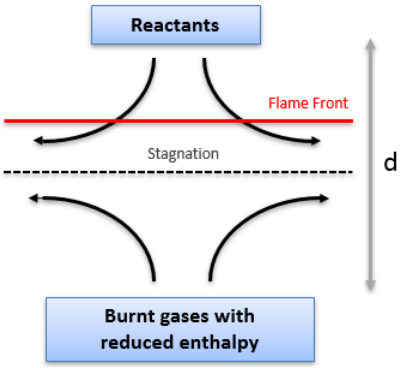

***Figure 3.6**: Laminar stretched premixed flame*

The flame thickness is obtained by using the temperature profile of an unstrained laminar flame at stoichiometric condition:

$$\delta_L^0 = \frac{T_2 - T_1}{\max\left(\left|\frac{\partial T}{\partial x}\right|\right)} \tag{3.35}$$

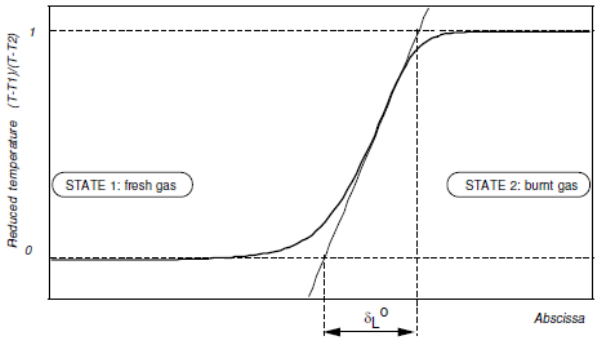

***Figure 3.7:** Defintion of flame thickness for a premixed flame*

The counterflows distance (*Figure 3.6*) can be set such as ~100÷150δ_L^0.

Once boundaries conditions are defined, the laminar flames are solved at the pressure and reactants temperature of interest. Each resolved flame was processed to evaluate the

laminar consumption speed by the integration of the heat release rate along the domain, Eq. (3.36):

$$S_c = \frac{1}{\rho_u \, (T_b - T_u)} \int \frac{Q}{c_p} \, dz \tag{3.36}$$

Where Q is the Heat release rate:

$$Q = \sum_{i=1}^{N} (h_i \, \frac{dc_i}{dt} \,) \tag{3.37}$$

with h_i species i partial molar enthalpy and $\frac{dc_i}{dt}$ the net production rate of species *i*.

3.4.2 Results and discussion

In this work, the designed process for calculation of consumption speed look-up table was applied to three different fuel mixtures:

- 100% CH_4: *Fuel A*
- 85%CH_4/15%C_2H_6: *Fuel B*
- 67%CH_4/33%H_2: *Fuel C*

for different strain rate and burnt temperature, varying equivalence ratio from Ø=0.4 to Ø=4.0, at relevant pressure and temperature replaying gas turbine typical operative conditions tested during the experimental campaign discussed in Chapter 2.

In *Figure 3.8*, the dependence of the consumption speed on strain rate and burnt gas temperature is shown for *Fuel A* and Ø=0.8. *Figure 3.9* shows a 3D representation of the same results.

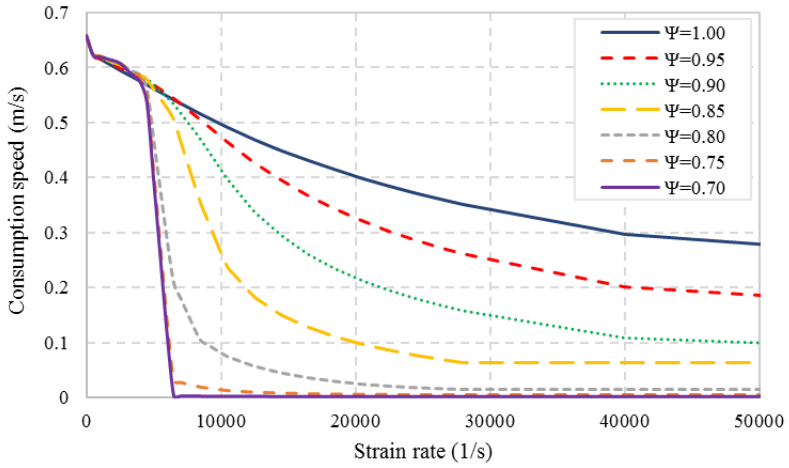

***Figure 3.8**: Consumption speed dependence on strain rate and burnt temperature, Φ=0.8*

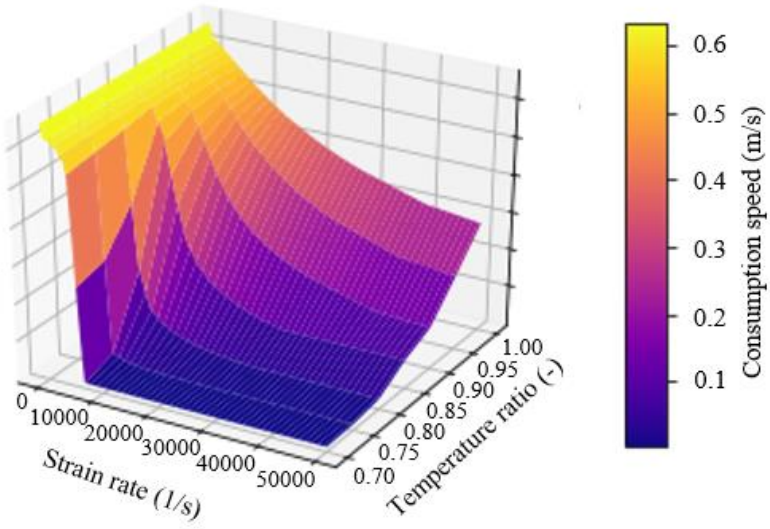

***Figure 3.9**: Consumption speed dependence on strain rate and burnt temperature, Φ=0.8*

For strain rate lower than 4000 1/s there is a very limited heat transfer from the reaction zone to the burnt side and the flame temperature reach the adiabatic value T_{ad} . This is evident since the consumption speed was not impacted by heat loss.

For higher strain, the consumption speed decrease with increasing strain showing a clear sensitivity to the presence of heat loss. For products temperature values above 1500K (ψ = 0.8) the consumption speed decreases reaching a minimum value on which it flattens up to very high strain values, without observing flame extinction. Otherwise, going below products temperature of 1500K and strain rate higher than 4000 1/s, a sudden decrease of the consumption speed was observed, indicating extinction of the flame. These behaviors have been also observed for different Ø. *Figure 3.10* shows the consumption speed trend for different equivalence ratios, the same results are reported in the *Figure 3.11* as a 3D distribution. The same tendency is shown also at various pressure e unburnt temperature, even if the curves are shifted to different values of consumption speed, *Figure 3.12*.

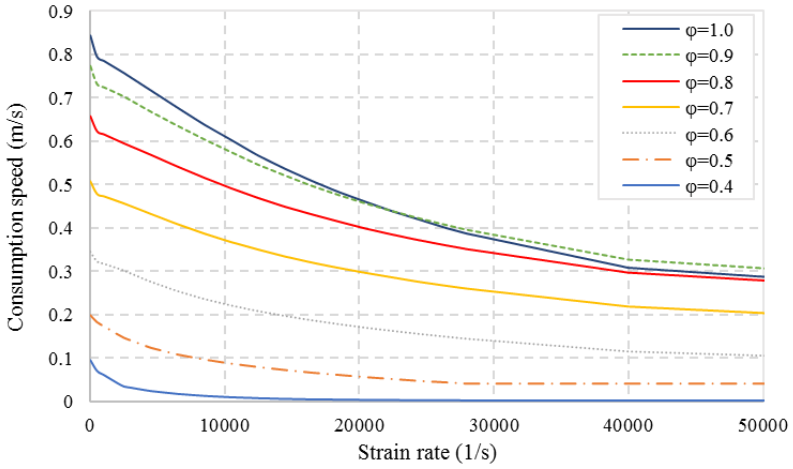

***Figure 3.10**: Consumption speed dependence on strain rate and equivalence ratio*

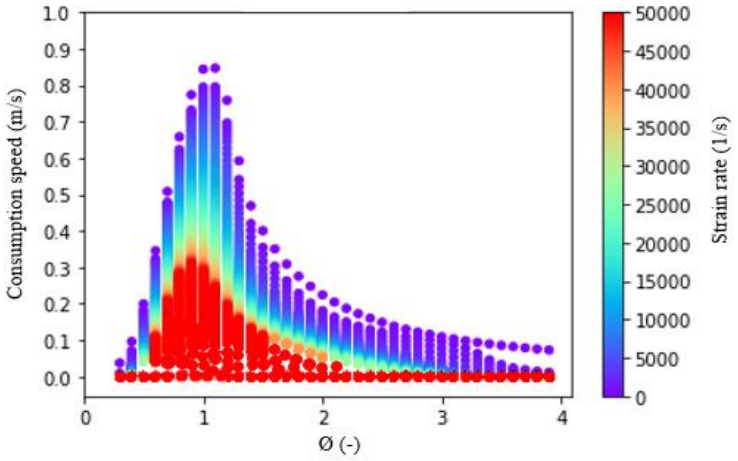

***Figure 3.11**: Consumption speed dependence on strain rate and equivalence ratio - 3D distribution*

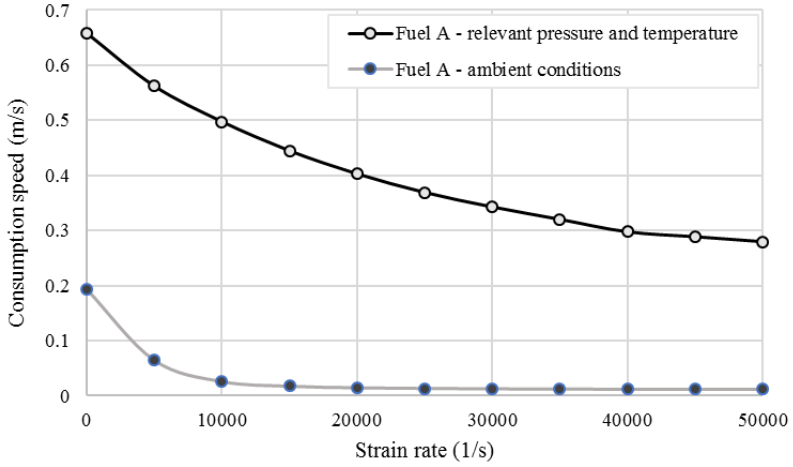

***Figure 3.12**: Consumption speed dependence on strain rate at different operating conditions*

The sensitivity of the consumption speed to fuel composition in shown in *Figure 3.13*. The consumption speed evaluated for *Fuel A* and *Fuel B*, for ϕ=0.8 at adiabatic condition is compared. As expected, the sensitivity of the consumption speed to fuel composition is evident, showing a difference of about 20% for any strain rate value. One implication of this result is that for a given strain field, such flame is more resistant to stretch level when

the ethane is added in the fuel mixture, impacting substantially, as shown in the next chapters, NO_X emissions and LBO.

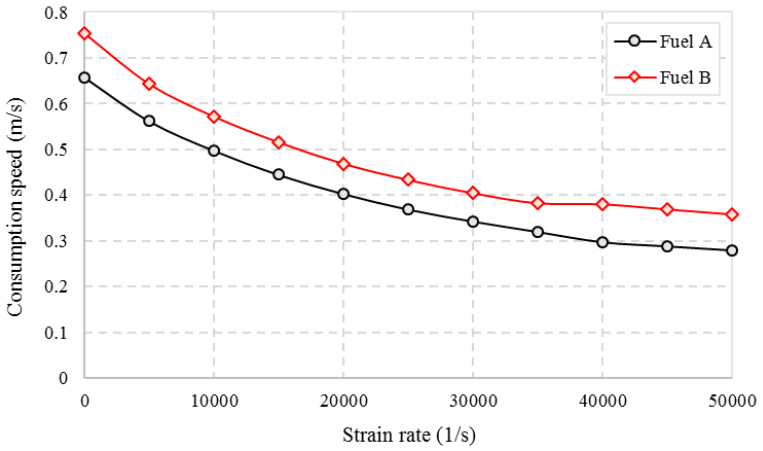

***Figure 3.13**: Consumption speed dependence on strain rate and fuel composition – Fuel A and Fuel B*

The effect of flame stretch is strongly dependent on preferential diffusion, dependent in turn on fuel composition, where differences in the relative rates of mass and thermal diffusion, usually expressed in terms of Lewis number, affect the local laminar flame speed and the tendency of the flame to become wrinkled. Therefore, the Le number becomes a critical parameter for stretch effect on flames. *Figure 3.14* shows a computation of Lewis numbers of main species for a premixed stoichiometric methane/air flame plotted versus spatial coordinate through the flame front [37].

For Le > 1 (*Figure 3.15*), as per CH_4/C_2H_6 fuel mixtures, the heat release decreases with increasing strain as soon as the flame is strained. Studies show that very large values of Le could lead to quenching. However, usual values of Le combustion chamber flames are never large enough to induce quenching [37].

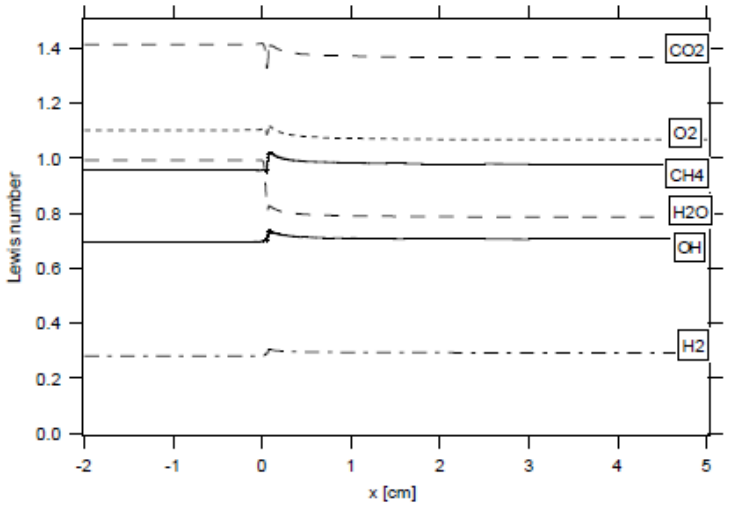

***Figure 3.14**: Variation of Lewis numbers of the main species in a stoichiometric laminar methane air flame*

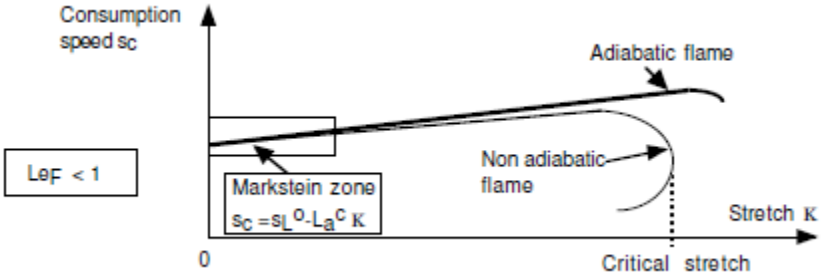

***Figure 3.15**: Effects of stretch on a laminar flame front at Le>1*

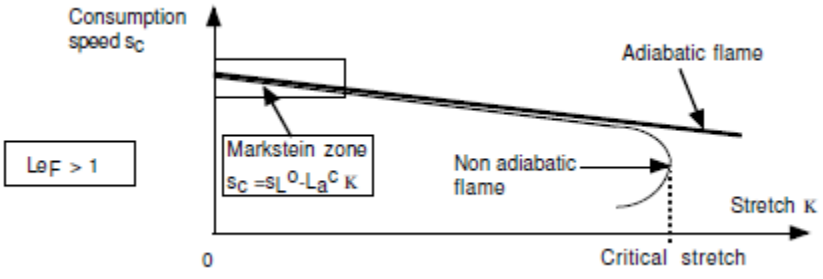

***Figure 3.16**: Effects of stretch on a laminar flame front at Le<1*

When Le < 1 (*Figure 3.16*), for low values of strain effects are observed: the consumption speed increases when strain increases. The increase of flame speed due to strain can be quite significant: a lean hydrogen-air flame can double its speed [37]. In the absence of heat loss, quenching is obtained only at very high stretch values. When the flame is not adiabatic, sudden extinction can be observed for lower strain rate levels.

Therefore, beside a consumption speed increase in absolute value, hydrogen blended to natural gas lead to a different flame behavior when stretched. In *Figure 3.17* is reported the consumption speed evaluated for *Fuel C*, for ϕ=0.8 at adiabatic condition, compared to *Fuel A*, showing the expected difference.

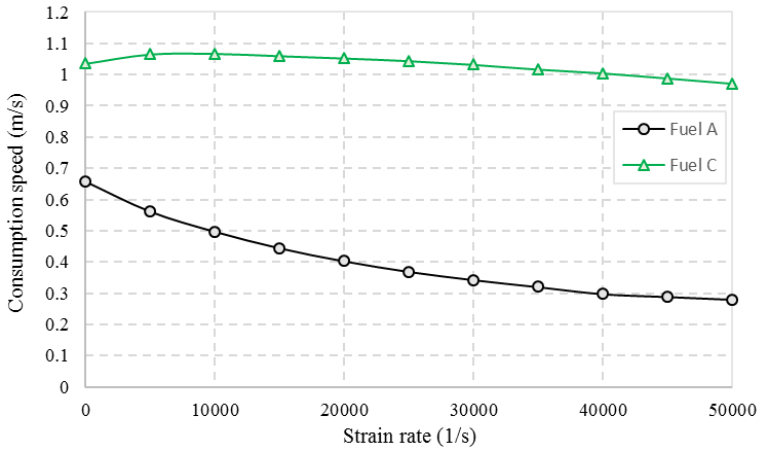

***Figure 3.17**: Consumption speed dependence on strain rate and fuel composition - Fuel A and Fuel C*

Hence, following this approach it is possible to calculate a three-dimensional look-up table to describe the dependence of consumption speed on equivalence ratio, strain, burnt side temperature and fuel composition. This allows to embed into CFD simulations the proper effect of fuel composition on flame response to strain. The results of this approach implementation are discussed in the next chapters.

4 Fuel composition effect on NOx emissions

This chapter describes the numerical simulations carried out, where an extended TFC model able to consider the combined effect of the strain and heat loss on the flame is implemented. The calculations are performed over three operating conditions of the flame and three fuel mixture compositions, for the comparison with NO_X experimental measurements presented in Chapter 2.

4.1 Numerical setup

The calculations reported hereafter were carried out with the CFD solver ANSYS® Fluent. The followed solution strategy for each simulated operating condition consists of:

- At first, RANS run to simulate a steady reactive solution.
- From converged RANS case the LES simulations are initialized and the unsteady flow field is calculated until a statistical steady solution is reached.
- Then, time averaged data from LES are extracted sampling approximately 0.2 s of physical time.
- Finally, NO_X formation is predicted in a postprocessing mode, with the flow field, temperature, and hydrocarbon combustion species concentrations fixed. Hence, only the NO equation is computed.

4.1.1 Computational domain

The computational domain, shown in *Figure 4.1*, is reduced to one single sector of the NovaLT16 entire combustion chamber with periodicity at the cut sides. The domain is made up of three fundamental parts: the Compressor Discharge Chamber (CDC), the burner and the combustion chamber.

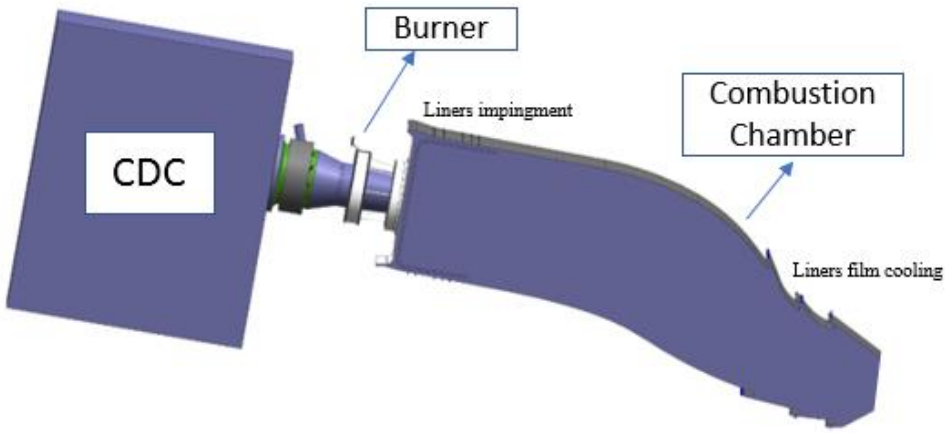

***Figure 4.1**: Computational domain*

A simplified geometry of the CDC was included in order to capture any flow distortion at the entrance of the premixer and to avoid any numerical interactions of the air inlet with the fuel injection inside the premixer. The combustor outlet was placed upstream the first stage nozzle throat and modelled as a pressure outlet with a constant static pressure. The latter value was retrieved from the test data to match the same Mach number in that section. The impingement and the film cooling of the liners were modelled as mass flow inlet to reduce as much as possible the overall cell count. Finally, a constant wall temperature has been imposed at the combustor wall, leveraging the available test data. This aspect is crucial to quantify the effect of the heat loss.

4.1.2 Mesh resolution

The mesh resolution plays a fundamental role in this kind of simulations. If the spatial discretization is not sufficient, the sub-grid contribution to the total strain rate becomes artificially high and can potentially lead to an unreal quenching of the flame brush specially when the combustor operates near the LBO conditions. So, it was decided to go beyond the Pope's criterion [52] [53], resolving up to 95% of the turbulent length scale in the primary zone of the combustor. This discretization was possible placing around 85 cells across the burner exit diameter. Moreover, an even higher resolution was achieved applying local refinements of the domain at the fuel injection locations and in the primary zone of the combustor where the flame gets stabilized. The mesh size is around 32 million poly mesh (*Figure 4.2*), requiring around 30.000 hours cpu-time per case. The time-step size was calculated in order to maintain the Courant number below the unit in the primary zone.

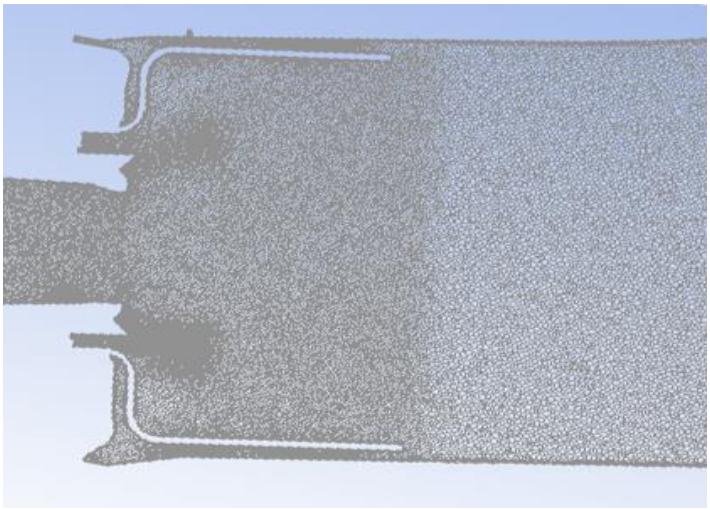

***Figure 4.2**: Mesh distribution*

4.1.3 Numerical scheme

The unsteady Navier-Stokes equation were solved with the Large Eddy Simulation approach using the solver Ansys Fluent® [54].

The sub-grid scale modelling was treated with the dynamic-stress closure of the Smagorinsky-Lilly model, to allow an adaptive estimation of Smagorinsky constant in time and space. The SIMPLE scheme was considered for the pressure-velocity coupling. Second discretization order was used for both spatial and implicit temporal discretization.

The combustion was simulated with non-adiabatic, compressible, diffusive flamelets based on the control variables of mixture fraction and progress variable. The progress variable source term was closed with ETFC presented in *section 3.3* reading in Fluent, by means of an UDF, the consumption speed look-up table computed for the different operating conditions and fuel compositions, shown in *section 3.4.2*.

4.2 NO_X emissions

4.2.1 NO_X emissions formation

The current approach to model NO production is solving the mass transport equation for the NO species, taking into account convection, diffusion, production and consumption of NO and the related species.

As thermal NO_X formation plays a dominate role in the whole different mechanisms, only thermal NO_X is considered in this work. The mechanism of thermal NO_X formation is based on the extended Zel'dovich mechanism [55], which consists of the following reactions governing the formation of NO from molecular nitrogen:

$$O + N_2 = NO + N \quad (4.1)$$

$$N + O_2 = NO + O \quad (4.2)$$

$$N + OH = NO + H \tag{4.3}$$

The net rate of formation of NO is given by:

$$\frac{d[NO]}{dt} = k_{f,1}[O][N_2] + k_{f,2}[N][O_2] + k_{f,3}[N][OH] - k_{r,1}[NO][N] - k_{r,2}[NO][O] - k_{r,3}[NO][H] \tag{4.4}$$

Where all concentrations are in $gmol/m^3$

In the above expression, $k_{f,1}$, $k_{f,2}$ and $k_{f,3}$ are the rate constants for the forward reactions (4.1) – (4.3) respectively and $k_{r,1}$, $k_{r,2}$, $k_{r,3}$ are the corresponding reverse rate constant. All of these rate constants are in $m^3/gmol - s$ and have been measured in numerous experimental studies:

$$k_{f,1} = 1.8 \times 10^8 e^{-38370/T} \qquad k_{r,1} = 3.8 \times 10^7 e^{-425/T}$$

$$k_{f,2} = 1.8 \times 10^4 T e^{-4680/T} \qquad k_{r,2} = 3.81 \times 10^3 T e^{-20820/T}$$

$$k_{f,3} = 7.1 \times 10^7 e^{-450/T} \qquad k_{r,3} = 1.7 \times 10^8 e^{-24560/T}$$

The forward rate constant for reaction (4.1) and the reverse rate constants for reaction (4.2) and (4.3) have large activation energies which results in a strong temperature dependence of NO formation rates. The activation energy for oxidation of N-atoms is small. When there is sufficient oxygen, as in a fuel-lean flame, the rate of consumption of free nitrogen atoms becomes equal to the rate of its formation and therefore a quasi-steady state can be established. This assumption is valid for most combustion cases except in extremely fuel-rich combustion conditions. Hence the NO formation rate becomes:

$$\frac{d[NO]}{dt} = 2k_{f,1}[O][N_2] \frac{\left(1 - \frac{k_{r,1}k_{r,2}[NO]^2}{k_{f,1}[N_2]k_{f,2}[O_2]}\right)}{\left(1 - \frac{k_{r,1}[NO]}{k_{f,2}[O_2]k_{f,3}[OH]}\right)} \tag{4.5}$$

The strong dependence of $d[NO]/dt$ on temperature is evident in the exponential term of equilibrium constants. In addition to concentration of stable species (i.e. O_2, N_2), the concentration of O-atoms and free radical OH have impact on thermal NO_X formation. In particular, results of some investigations [56] suggest that in turbulent flame the effect of O-atoms on the NO_X formation rate is more significant.

4.2.2 NO_X emissions results

At equivalent operative condition of ISO-base load of the gas turbine, three different fuel compositions have been simulated. In detail, the numerical setup described in *section 4.1* has been applied to three different flame conditions varying fuel pilot split (keeping constant the total fuel mass flow rate), comparing the usual Zimont TFC model and the Extended TFC with the test results.
In the *Table 4.1* below, a summary of the simulated conditions is reported:

Fuel composition	**Operative condition**
Fuel A	1.0, 1.4, 1.6 normalized pilot split
Fuel B	1.0, 1.4, 1.6 normalized pilot split
Fuel C	1.4, 2.0, 2.8 normalized pilot split

***Table 4.1**: Simulated conditions*

In order to be able to predict with reasonable accuracy the NO_X emissions, the defined setup should be able to capture as much as possible not only the single flame conditions but also the NO_X emissions trend approaching the lowest value.

A general overview of the results is reported in *Figure 4.3*. Here the numerical results of both the standard approach implemented in Ansys Fluent® and the strained formulation are compared with the test. The entire set of data is normalized against the experimental measurements for pure methane at the lowest pilot split.

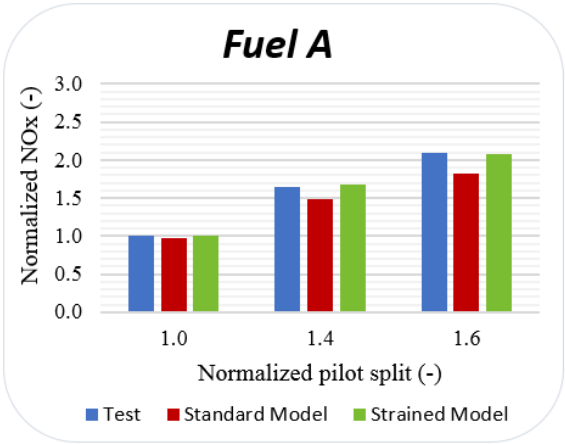

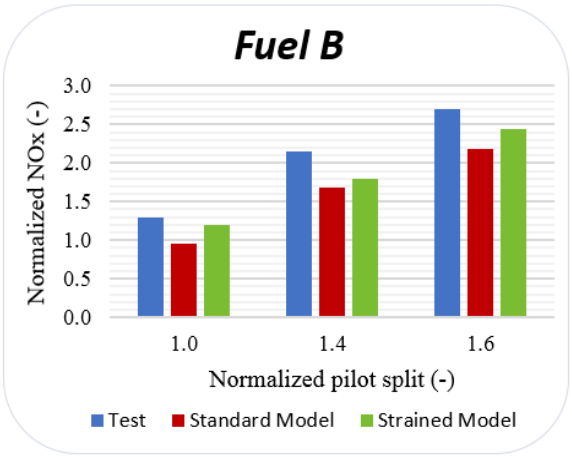

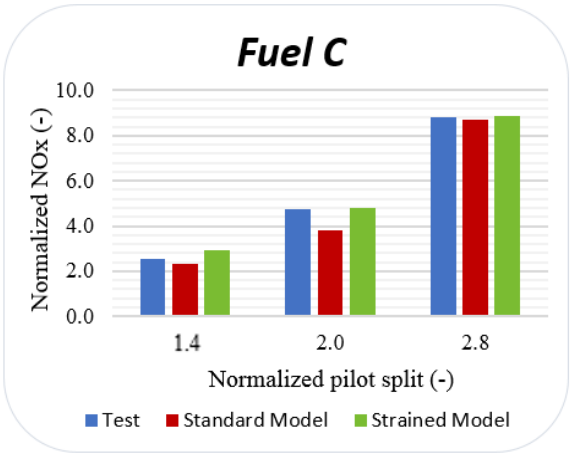

***Figure 4.3**: Numerical vs experimental data*

The main results in terms of NO_X emission can be summarized as follows:

- The standard model generally underpredicts the NO_X emission independently by the blend. Nevertheless, that approach produces larger error when the C_2H_6 or H_2 is added to the blend. For this reason, an alternative approach has been investigated.
- Both the formulations are able to capture the emissions trend increasing the piloted amount of fuel. But, only applying the strained formulation, the different fuel composition seems to significantly act in the right direction, i.e. providing higher NO_X emission with *Fuel B* than *Fuel A* for each value of pilot split considered.
- Regarding the new formulation, the NO_X emissions are always higher than the standard model. This leads to a very high limitation of the error with the test data with pure methane and to a recovery of the discrepancy with the test points having ethane or hydrogen content. In absolute terms, the residual difference is quite small since in this condition the combustor is approaching the single digit emission level.

4.2.3 Extended TCF application impact

Focusing on *Fuel B* at normalized pilot split equal to 1.0, the analysis of the thermal fields permits to point out the differences predicted by the standard model and the strained formulation. *Figure 4.4* shows the temperature contour on a plane passing through straight holes of the piloted fuel line. Even if the morphology of the flame is similar, two differences can be detected:

- As expected by the use of unstrained laminar flame speed, the flame predicted by the standard model is shorter in the core region where the process is mainly occurring starting from premixed conditions.
- The strained thermal field shows that a higher temperature peak occurs, downstream of the pilot injections region, with respect to the standard model

characterized by a quite uniform temperature distribution along the axis of the combustor.

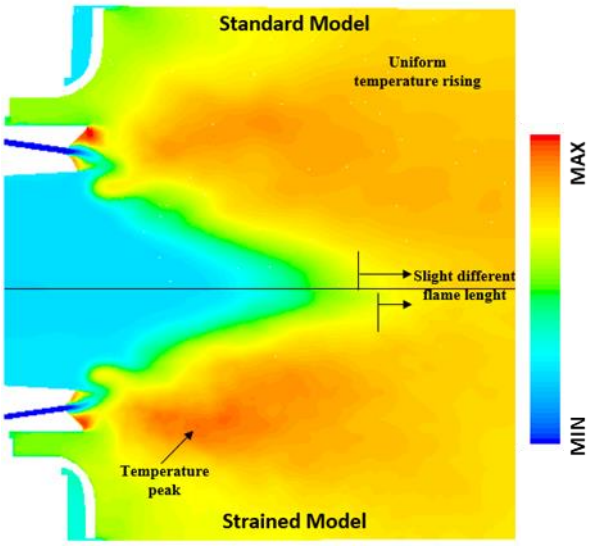

***Figure 4.4**: Standard (Top) vs Strained (Bottom) thermal field for Fuel B*

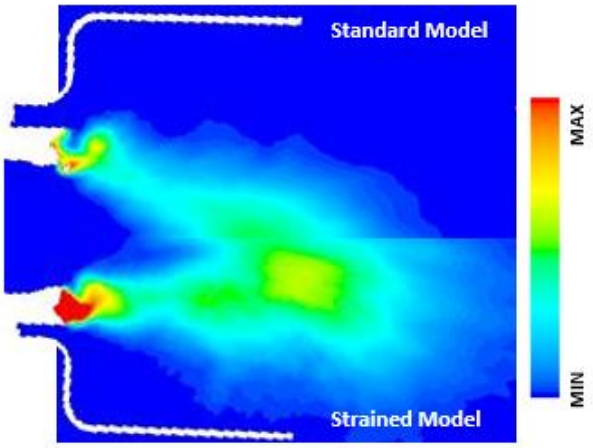

***Figure 4.5**: Standard (Top) vs Strained (Bottom) O-species mass fraction field for Fuel B*

More important, the concentration of O-species is predominant in strained model, as shown in *Figure 4.5*. The overlap of the higher temperature value and O-concentration in

the primary zone leads to an increase in NO_X emissions when strained formulation is adopted.

Also, the difference in the velocity fields seems to play a key role. *Figure 4.6* reports the contours of the axial velocity on the mid-longitudinal plane of the combustor; in this plot the iso-line is set at the stagnation points helping to identify the recirculation regions inside the domain. It is evident that in the outer side of the combustor, the strained flame is characterized by a larger recirculation zone as well as in the inner side, this lead to increase the residence time of the reactants in the primary zone boosting the NO_X formation process. This effect is related to a larger curvature of the swirling flow compared to the standard model.

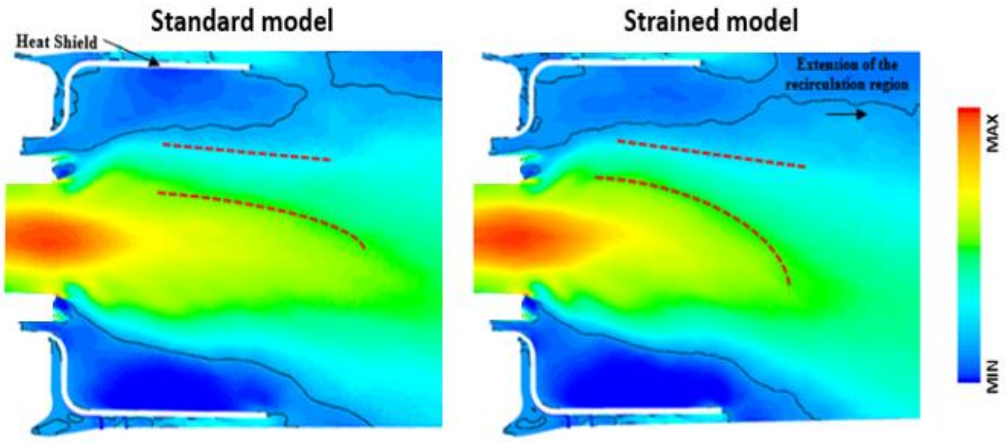

***Figure 4.6**: Standard (Top) vs Strained (Bottom) axial velocity*

An important aspect of including the strain rate into the solution is the possibility to verify the interaction between the air flow coming from the premixer with the pilot fuel line. In this sense, *Figure 4.7* clearly describes the aero-dynamic in this critical region of the combustor showing the resolved strain rate field close to one of the pilot hole. It is evident how the fuel is delivered in a region where the strain rate is maximum, weakening the stability of the flame.

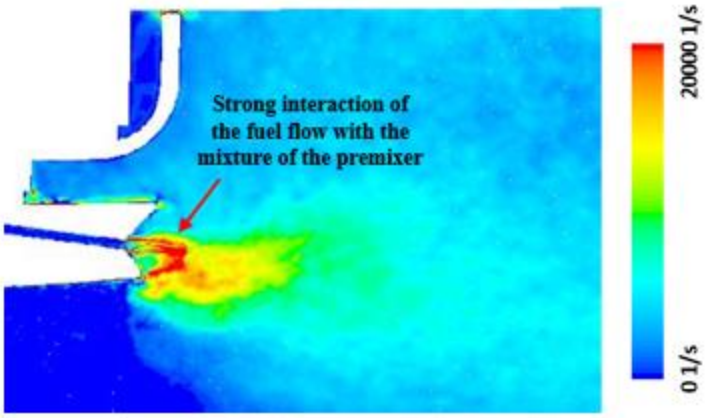

***Figure 4.7**: Time averaged resolved flame strain rate contour*

From the analysis of the strain fields it has been verified that the sub-grid strain rate is an order of magnitude lower than the resolved part, *Figure 4.8*. So, it has not been included in the post-processing that will be presented in the following sections. The same can be stated for the heat-loss (*Figure 4.9)*: despite realistic temperature distributions have been imposed on the combustor walls (leveraging the test data), its effect is negligible and burnt temperature is almost equal to equilibrium temperature in the whole computational field. For the sake of simplicity, although included onto the global solution, will not be further discussed of this effect.

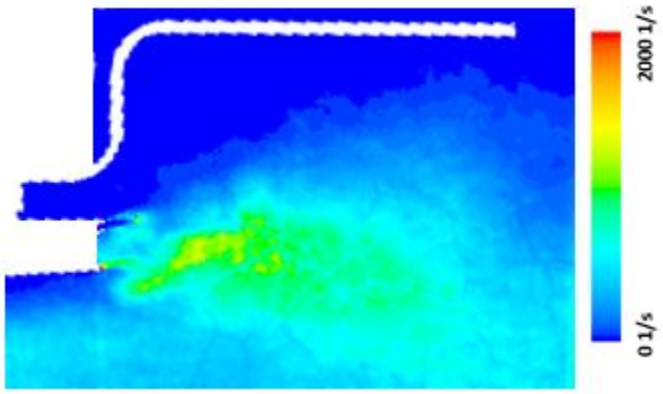

***Figure 4.8**: Time averaged sub-grid strain rate contour*

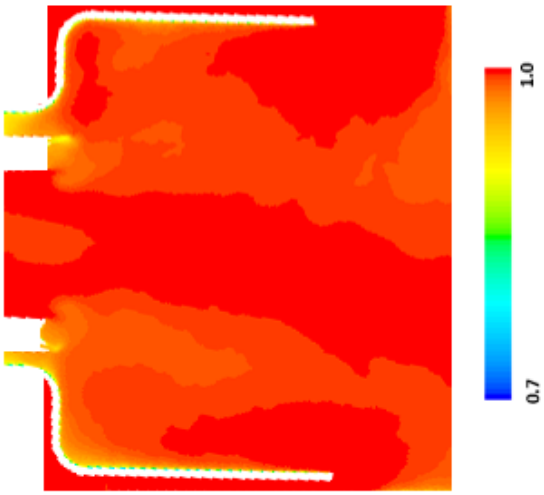

***Figure 4.9**: Time average contour of heat loss parameter Ψ*

4.2.4 Fuel composition effect

In this section, the results of numerical analysis carried out using the ETFC strained formulation comparing the three different natural gas mixtures are presented.

Focusing on value 1.4 of normalized fuel pilot split, mean axial velocity contours on a plane passing through holes of the piloted fuel line are shown in *Figure 4.10*. Flame shape is evidently influenced by different composition and a more extended recirculation zone on both inner and outer side are established with *Fuel B* and *Fuel C*. This is due to differences in flame stabilization process influenced by ethane and hydrogen contained in the fuel mixture.

Fuel composition effect is also valuable on thermal, strain and consumption speed fields shown on the mid-longitudinal plane of the combustor.

Fuel B with respect to *Fuel A*, in *Figure 4.11*, shows wider regions at high temperature and a peak downstream the pilot injection producing higher NO_X emissions according with experimental tests. This behavior is even more evident when hydrogen is in the mixture,

as for *Fuel C*, showing an increase in flame adiabatic temperature, that inevitably results in an exponential increase of NO_X emissions. The results, shown below, also prove high diffusion ability of H_2 revealed in the flame shape.

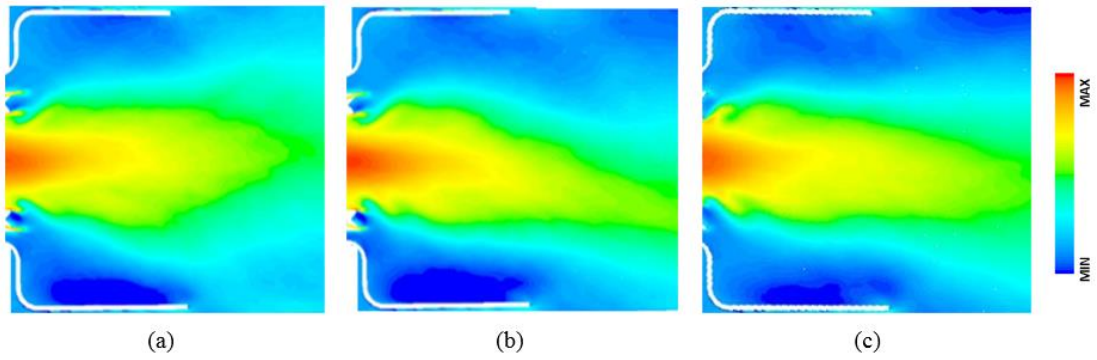

***Figure 4.10**: Mean axial velocity contour at pilot holes cross plane: (a) Fuel A, (b) Fuel B, (c) Fuel C*

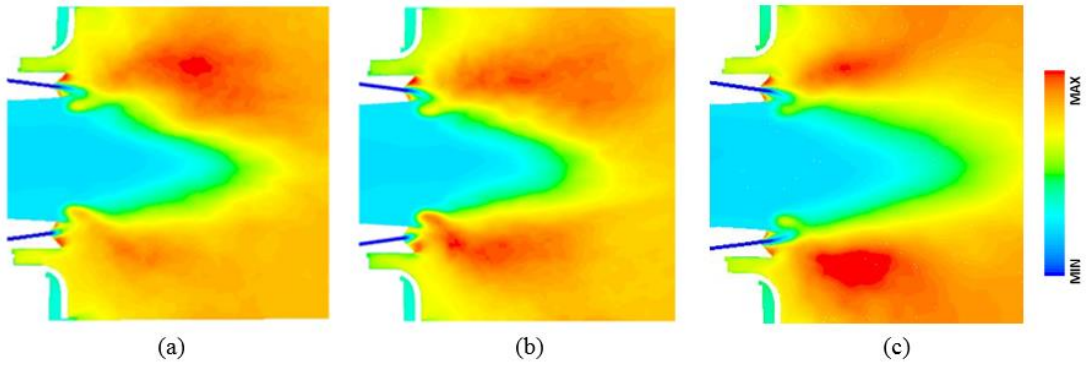

***Figure 4.11**. Mean temperature contour: (a) Fuel A, (b) Fuel B, (c) Fuel C*

The three cases, simulated at the same operating condition, are characterized by similar fields of resolved strain reaching peak values just downstream the pilot holes injections. This means that, for the same strain rate, the ethane percentage in mixture causes an increase of 20% in consumption speed and the hydrogen addition raises the burning velocity by approximately 2.2 times.

The consumption speed fields, in *Figure 4.12*, prove that the *Fuel B* flame is more resistant to high strain level with respect to *Fuel A*. So, with the ethane content the flame gets stabilized closer to burner exit and it is more stable allowing to extend the operability limits.

This effect become even more evident using *Fuel C* being characterized by higher field of laminar consumption speed.

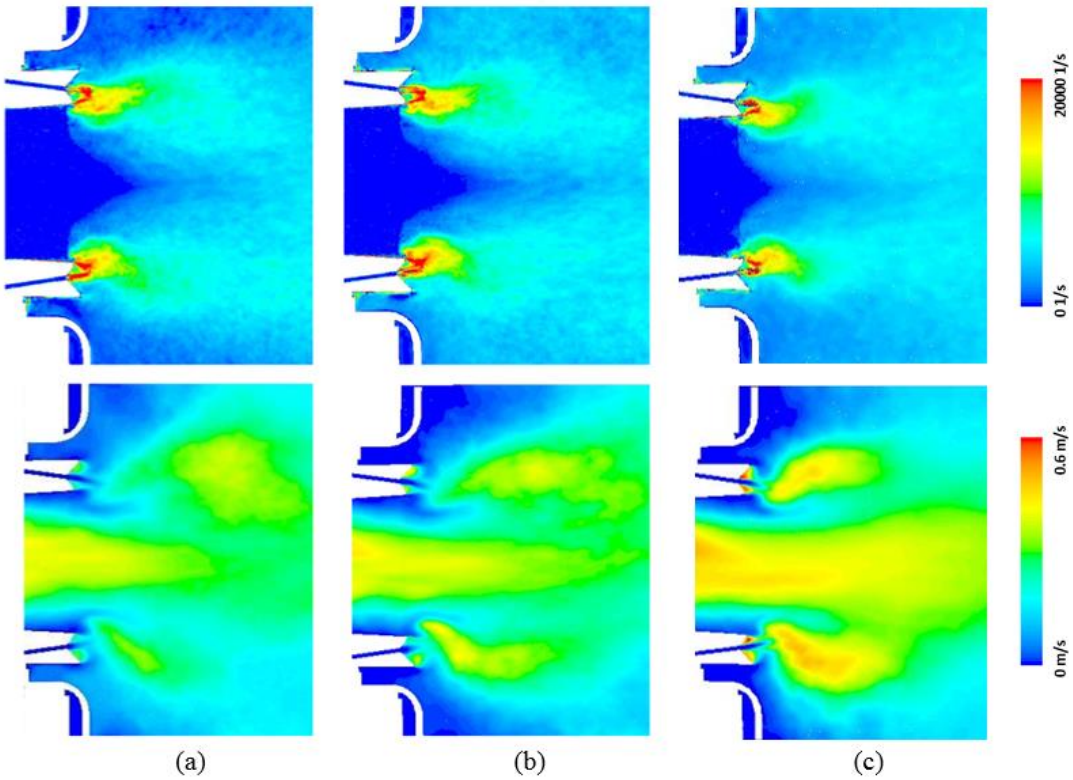

***Figure 4.12**: Mean resolved strain (Top) and consumption speed contour (Bottom): (a) Fuel A, (b) Fuel B, (c) Fuel C*

This behavior is also confirmed by flame lift-off height. Focusing on *Figure 4.13*, where the flame front is identified by the iso-progress variable surface at 0.8 and colored by temperature, it is evident that flame is well anchored to pilot injection exit holes when ethane or hydrogen in present in the mixture while is substantially stretched in case of pure methane resulting in a longer flame morphology. The increase in the laminar burning velocity was identified as the main factor that affects the height of the flame.

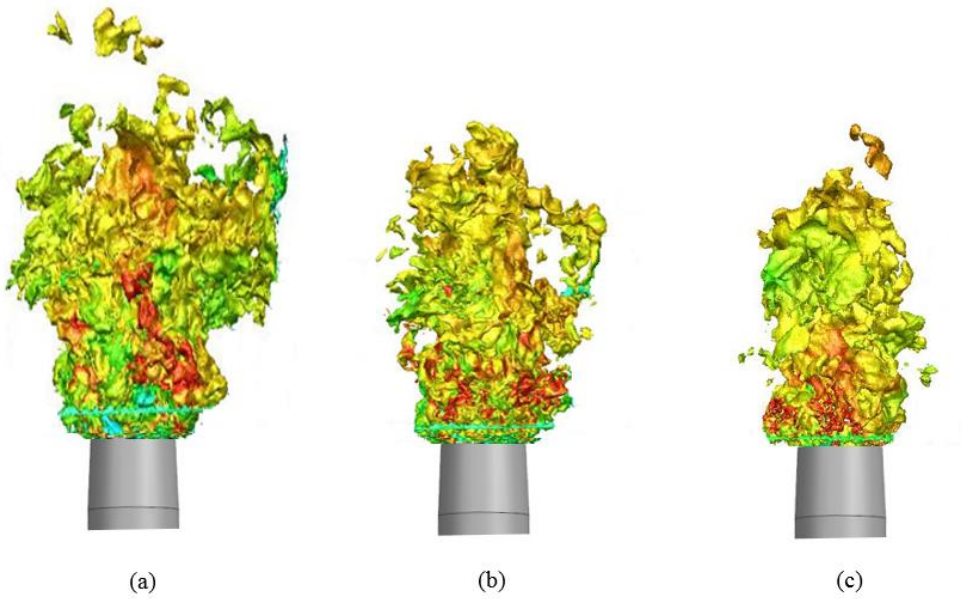

***Figure 4.13**: Flame front identified by iso-progress variable surface and colored by temperature*

The ETFC model, including stretch and heat loss contributions, proved to be particularly suitable to capture change in flame behavior on fuel composition variation showing large potential to predict the operability region according to the fuel.

For this purpose, for the prediction the extinction mechanism that bring to lean blow-out it has been applied in the next Chapter.

5 Fuel composition effect on LBO

Nowadays, one of the primary requirements of a gas turbine combustor is that this must be able to run over a wide range of operating conditions keeping low emissions and achieving fundamental stability prerequisite. In order to identify the conditions where the machine can operate safely, without the risk that the flame extinguish, it is necessary to determine the stability curve of the combustor. The term stability is used to describe the range of fuel/air ratios over which stable combustion can be achieved before flame extinction occurs. The stability performance of a combustor are typically determined by performing a series of extinction tests at constant levels of inlet air temperature and pressure [55]. After igniting the mixture, the fuel flow is gradually reduced until flame extinction occurs. The fuel and air flows at this event is registered as lean blow-out point. If the lean blow-out limit is accurately identified, it is possible to obtain leaner conditions, reduce the temperatures in the combustion chamber and contain the NO_X emissions. In this view, the accurate lean blow-out prediction represents a valuable instrument to identify the boundaries of the stable operating region, reducing as much as possible the pollutant emissions.

During design phase of the combustion system, having an accurate model to predict the blow-off inception would reduce expensive test campaigns and would allow to explore different development opportunities of fuel burner able to emissions reduction while maintaining a sufficiently wide stable operation window for different fuel mixture. Indeed, the natural gas composition variation requires testing of gas turbine combustor to evaluate the fuel performance on combustion stability. Fuel composition affects physico-chemical

processes impacting the flame response when quenched as in the extinction mechanism happens.

The development of CFD tools to better describe these fuel effects in realistic configurations is thus crucial in complementing experiments and reducing cost and duration. During the years, experiments supported also the development of semi-empirical correlations to relate LBO criteria to equivalence ratio and other operating conditions, however, not including turbulence-chemistry coupling reduces their robustness and prediction capability.

The CFD simulation of lean blow-off still represents a challenge, since requires the use of combustion models that address the flame extinction mechanisms e and the adequate simulation of the highly transient combustion near the extinction limit.

In this work, LES simulations are performed on the same computational domain described in *section 4.1.1* applying the extended TFC model that includes the stretch and heat loss effects, fundamental to accurately capture LBO.

LES results obtained for a pure methane mixture have been compared to available experimental data to assess the model capability in reproducing observed phenomena. Thereafter, the same numerical setup and process have been applied to examine the LBO performance for a methane-ethane fuel mixture in order to predict the LBO-limit in terms of equivalence ratio and identify the fuel effect on the blow-out behavior.

5.1 Experimental diagnosis and findings

The combustor operating conditions considered for the LBO investigation are at 50% ISO load, fully representative of the engine behavior.

Two kind of measures, whose acquired during the FAR test campaign, have been used for LBO detection:

- flame intensity, measured in the primary zone of the combustor by flame detectors;
- pressure pulsations, measured by means of pressure probes that can capture some precursors acoustic tones of LBO.

In the experimental test, after igniting and stabilizing the mixture at conditions far from the blow-off limit, the blow-off of the flame was induced with a gradual reduction of pilot split flow rate weakening the piloted stabilization region and keeping the overall temperature constant. This means that global equivalence ratio of the mixture remains constant, hence decreasing in the pilot region where the flame gets stabilized and the most of NO_X emissions are produced. Moreover, flame approaching blowoff tends to oscillate between extinction and re-ignition phases. For this reason, blowoff in many systems is preceded by a growing amplitude of low frequency oscillations, used to provide a warning that blowoff is being approached.

Table 5.1 shows the experimental conditions for *Fuel A* and *Fuel B*, in terms of pilot split, considered for this investigation. The data have been normalized against the value of the stable point for both fuel mixtures.

Fuel composition	**P_s/P_{s0} =1.0**	**P_s/P_{s0} =0.8**
Fuel A	Stable	LBO
Fuel B	Stable	Stable

***Table 5.1**: Operating conditions investigated experimentally*

When the combustor run with *Fuel A*, a pilot split reduction of 20% is necessary to extinguish the flame. Instead, with *Fuel B* the LBO was not encountered experimentally and it have been simulated numerically and reported hereafter.

5.2 Numerical results

The numerical investigation stars simulating the stable conditions for 10 Flow Through Times (FTTs). From well-developed LES results, the fuel mass flow rate of pilot is reduced of steps $\Delta Ps=20\%$.

5.2.1 Fuel A

For *Fuel A*, the stable condition has been simulated according to the *Table 5.1*. Starting from this condition the pilot mass flow rate has been decreased up to $0.8*Ps_0$, the flame started showing a flickering behavior and, after a delay time, a constant decreasing of its reactivity was observed leading to the blow-out point.

During the simulations the instantaneous quantities of temperature, product formation rate (PFR) and OH mass fraction are volume-averaged in the chamber and monitored to analyze their evolution during the blow-off transient. The results are reported in *Figure 5.1*.

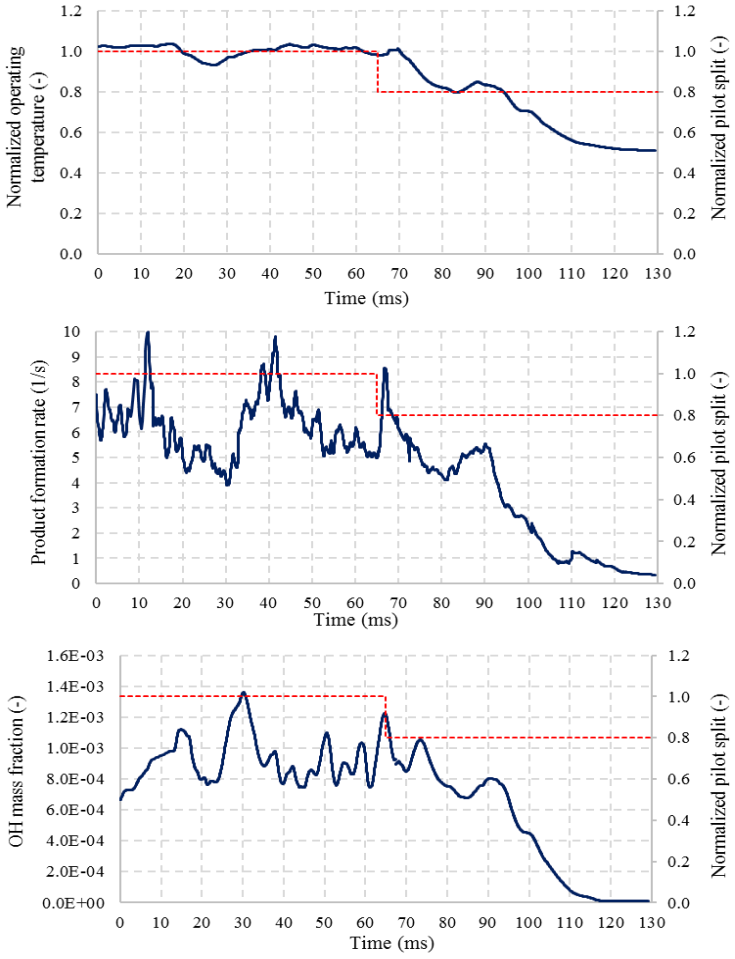

Figure 5.1: *Time series of volume-averaged quantities in combustion chamber during blow-off transient for Fuel A. The dotted line represents the normalized pilot split value over time*

The averaged variables present different behaviors over time. The PFR oscillates much more than temperature, that changes smoothly for its dependence on the entire flow field. Instead, the OH mass fraction, that shows the transition zone from unburned to burnt gas, presents an unsteady behavior characterized by slower fluctuations with respect to PFR. As can be seen, after the changing of boundary conditions at burner inlet, there is a delay of about 25-30ms in the response of these variables that corresponds to the time needed to the information to flow from the burner to the chamber and the system tries to get stabilized at a new operating condition. Then, temperature, product formation rate and OH, influenced by the leaner conditions in the region of flame stabilization, decreases rapidly up to the blow-off event. The loss of flame is recognized since the temperature at the outlet section of the combustor reaches about the compressor discharge temperature.
These results indicated that the LES using the ETFC model is able to adequately reproduce the blow-off dynamic showing to be in good agreement with experimental data, detecting the same LBO point. Therefore, the same approach has been used to estimate the LBO limit for *Fuel B*, since is expected to be sensitive to fuel composition and experimentally up to P_s/P_{s0} =0.8 it was not encountered.

5.2.2 Fuel B

The composition impact on fuel properties contributes to change the relative LBO-limit. The strong dependency to flame response to quenching phenomena needs the application of detailed models able to capture the differences between the investigated fuels.
The same LES setup used for *Fuel A* has been applied to *Fuel B*, considering the proper effect of ethane content on consumption speed look-up table generation. Starting from the last stable point identified during the experimental test, LBO is triggered by progressively reducing pilot fuel flow rate. The followed process and achieved results are summarized in *Table 5.2*:

Fuel composition	**P_s/P_{s0} =1.0**	**P_s/P_{s0} =0.8**	**P_s/P_{s0} =0.6**	**P_s/P_{s0} =0.4**
Fuel B	Stable	Stable	Stable	LBO

***Table 5.2**: Operating conditions investigated numerically for Fuel B*

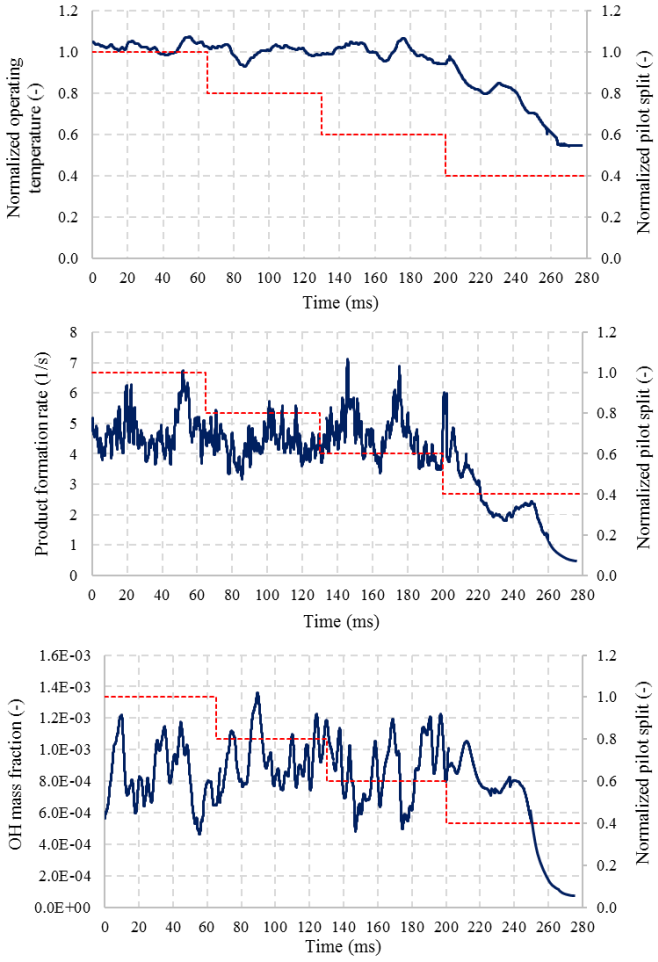

***Figure 5.2**:Time series of volume-averaged quantities in combustion chamber during blow-off transient for Fuel B. The dotted line represents the normalized pilot split value over time*

As showed in *Figure 5.2* by the volume-averaged values, up to P_s/P_{s0} =0.4 all the quantities do not respond clearly to the step reduction of pilot fuel rate maintaining similar behavior. In the last step, after 40ms the flame decrease its reactivity leading to LBO.

Moreover, it was numerically verified that the flame could blow off even later, decreasing the pilot by smaller step. Because ethane content lends the flame insensitive to smaller perturbations.

Figure 5.3 shows some instantaneous contour plots of temperature and progress variable during the transient phase. The flame is well anchored to the burner exit within the first 40 sec after the last pilot split change, its shape and structure do not change significantly. As soon as the leaner flow gets through the pilot line to the recirculation zones, leading to local extinctions where the strain is higher, the flame starts losing its strength and anchoring at the pilot region direct towards the loss of flame. This is due to the progressive leakage of fresh reactants across the flame front into the recirculation zone where the mixture is leaner. The flame attempts to adapt to the leaner condition in a first phase but shortly is subjected to strong fluctuations and its structure is significantly affected by the turbulence, as also confirmed by progress variable evolution. The flame is progressively disintegrated and rapidly moves to blows off. This behavior is confirmed by the rapid decay of PFR and OH after the 240 ms.

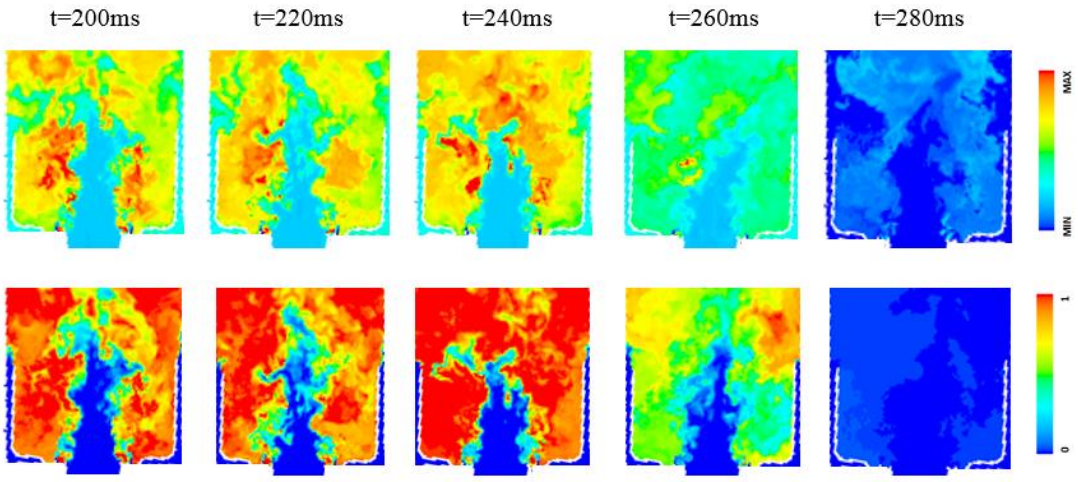

***Figure 5.3**: Time evolution leading to loss of flame for Fuel B. Temperature (Top) and progress variable (Bottom)*

These results prove also the impact of fuel composition, indeed ethane content in natural gas leads to enlarge the burner operating window with respect to a pure methane mixture,

since the stronger resistance to flame quenching allows to get stabilized in high strain region and consequently to operate with lower pilot split values resulting in a global reduction of NO_X emission.

To further describe the impact of fuel composition on loss of flame, *Figure 5.4* reports two different scatter plots for both fuel mixture *Fuel A* and *Fuel B* approaching the LBO. The top row of the graph reports the temperature while the bottom one the resolved strain rate colored by temperature both as a function of mixture fraction. The temperature distributions against the mixture fraction highlight that the flame is close to the blow off, indeed the points distribution is collapsed to very lean value of mixture fraction, lower than 0.025, and low temperature value where the flame is no longer sustainable.

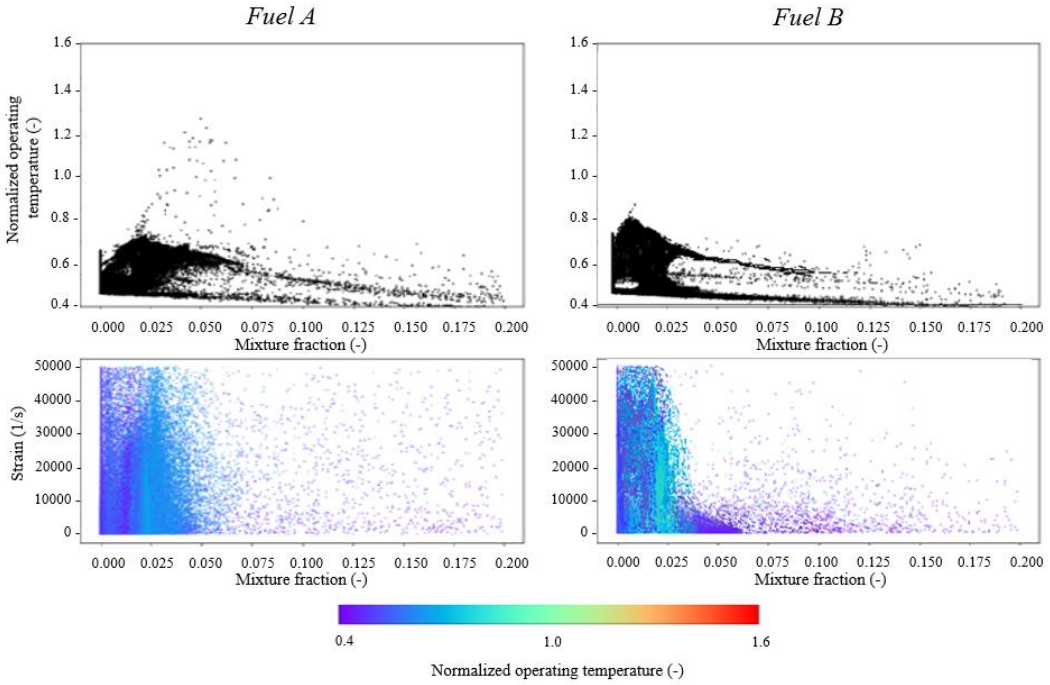

***Figure 5.4**: Temperature (Top) and resolved strain (Bottom) as a function of mixture fraction on a reference plane. In the bottom graphs the scatter points are colored by temperature*

Analyzing the second bottom row of the picture, it is clear that, although the two flame are overall subjected to similar level of strain rate since the mass flow rate is substantially the same, *Fuel B* approaching the LBO is characterized by a portion of points distribution of

the fluid domain at higher temperature with respect to *Fuel A*. This can be explained considering that, under the same strain conditions, *Fuel A* is characterized by a lower consumptions speed and, therefore, flame resistance, exhibiting a faster rate of decay.

6 Conclusions

In this work, the effects of natural gas composition on the operation of low NO_X burners employed in combustion chamber for heavy-duty gas turbine have been investigated with the aim to address the impact of composition variation on operability and emissions of lean premixed combustion system. This is a topic of growing interest as these systems operate close to the edge of combustion stability to reduce emissions of NO_X and even modest upsets in operating conditions, including those related to variation in fuel composition, could become intolerable.

Despite natural gas is mainly associated to methane, its constituents may vary containing methane between 60–99%, ethane and some other higher-order hydrocarbons (C_2+) for the remaining composition percentage. Furthermore, in a renewable generation landscape, hydrogen integrated with natural gas become a possible scenario to be verified with the current technology. Because of the mixture properties change it is important to gain more understanding of the impact of fuel composition on the combustion system performance.

This work is an attempt to address observed behaviors during experimental test campaign of a combustion chamber for a heavy-duty gas turbine, under elevated operating temperature and pressure, improving the predictive capacity of CFD analysis of fuel composition effects. An accurate tool sensitive to fuel composition could be used since the preliminary design phase of combustion system allowing to reduce expensive test.

However, it is matter of fact that fuel composition affects the laminar flame speed and the flame resistance to stretch playing an essential role in determining NO_X emissions, LBO margin and combustion dynamics.

Nevertheless, widely used combustion models for industrial applications do not properly consider some effects such as the local quenching due to stretch at which the flame front is subjected and that directly impacts the turbulent flame speed. Moreover, the effect of flame strain is particularly sensible to the local heat loss, which should be also taken into account. For these reasons this work introduces a strained formulation of combustion model integrating the effect of strain and heat loss, and consequently their fuel-dependence, in LES framework. Therefore, these effects have been embedded in the combustion modelling replacing the unstrained laminar flame speed used to calculate the turbulent velocity in the Zimont TFC model with the laminar consumption speed. The latter is calculated by computing asymmetric counterflow strained premixed flamelets, for a given operating condition and gas composition and integrated in CFD analysis by means of a Fluent UDF.

For a gas turbine real operating conditions and three natural gas compositions, the consumption speed was calculated as function of equivalence ratio, strain and heat loss obtaining a 3D look-up table used as input to the combustion model. This work represents the first application to real gas turbine flames and fuel blends. A scale resolving CFD analysis have been performed for an annular combustor sector at different operating conditions, showing promising results compared against available experimental data in terms of NO_X emissions and LBO prediction. The key findings of this study are highlighted below:

- The ETFC strained formulation, implemented within LES framework over three flame conditions, demonstrated high capability to describe fuel composition effect on flame behavior thanks to the inclusion of the flame stretching, capturing the emissions trend when the piloted amount of fuel increase and leading to a very high limitation of the error with the test data approaching the single digit emissions.

- This setup showed the ability to capture the main evolution of the flame allowing a great prediction of the flame structure approaching blow-off. The sensitivity to fuel composition of blow-off inception has been captured with good accuracy.

In conclusion, this work gives an overview of the possible development area for studying fuel gas composition impact on combustion system operability showing promising fundamentals for the characterization of the flame behavior of fuel blends with varying composition.

Bibliography

[1] International Energy Agency, "World Energy Outlook 2019 - Executive Summary," 2019.

[2] British Petroleum, "BP's Energy Outlook," 2019.

[3] "Natural Gas Composition," [Online]. Available: https://www.croftsystems.net/oilgas-blog/natural-gas-composition.

[4] Internationa Energy Agency, [Online]. Available: https://www.iea.org.

[5] Lieuwen, T., McDonell, V.G., Petersen, E., Santavicca, D., "Fuel Flexibility Influences on Premixed Combustor Blowout, Flashback, Autoignition, and Stability," in *ASME Turbo Expo 2006, GT2006-90770*, Barcelona, Spain, 2006.

[6] Bougrine, S., Richard, S., Colin, O., Veynante, D., "Fuel Composition Effects on Flame Stretch in Turbulent Premixed Combustion: Numerical Analysis of Flame-Vortex Interaction and Formulation of a New Efficiency Function," *Flow, Turbulence and Combustion*, vol. 93, pp. 259-281, 2014.

[7] Abbot, D.J., Bowers, J.P., James, S.R., "The impact of natural gas composition variations on the operation of gas turbines for power generation," in *The Future of Gas Turbine Technology 6th International Conference*, Brussels, Belgium, 2012.

[8] Romano, S., Cerutti, M., Riccio, G., Romano, C., Andreini, A., "Effect of natural gas composition on low NOx burners operation in heavy duty gas turbine," *Journal of*

Engineering for Gas Turbine and Power, vol. 141, pp. 114501-11-8, vol. 141, no. 11-8, p. 114501, 2019.

[9] Roby, R.J., Klassen, M.S., Vashishat, D., Joklik, R., "Effect of Fuel Composition on Gas Turbine Operability and Emissions," *Combustion Science & Engineering, Inc*, 2001.

[10] Flores, R.M., McDonell, V.G., Samuelsen, G.S., "Impact of ethane and propane variation in natural gas on the performance of a model gas turbine combustor," *Journal of Engineering for Gas Turbines and Power*, vol. 125, no. 3, 2003.

[11] Lee, John C. Y., "Reduction of NOx Emission For Lean Prevaporized-Premixed Combustors," 2020.

[12] Hack, R. L. and McDonell, V. G., "Impact of Ethane, Propane, and Diluent Content in Natural Gas on the Performance of a Commercial Microturbine Generator," *Journl of Engineering for Gas Turbines and Power*, vol. 130, 2008.

[13] Figura, L., et al, "The Effects of Fuel Composition on Flame Structure and Combustion Dynamics in a Lean Premixed Combustor," in *ASME Turbo Expo*, Montreal, Canada, 2007.

[14] Gonzalez-Juez, E.D., Lee, J.G. and Santavicca, D.A., "A Study of Combustion Instabilities Driven by Flame-Vortex Interactions," in *1st AIAA/ASME/SAE/ASEE Joint Propulsion Conference*, 2005.

[15] Russ, M., Meyer, A. and Büchner, H., "Scaling Thermo-Acoustic Characteristics of LP and LPP Swirl Flames," in *ASME Turbo Expo* , Montreal, Canada, 2007.

[16] Ferguson, D., Richards, G.A. and Straub, D., "Fuel Interchangeability for Lean Premixed Combustion in Gas Turbine Enginers," in *ASME Turbo Expo*, Berlin, Germany, 2008.

[17] Lieuwen, T., Emerson, B., Perullo, C., Sheppard, S., Kee, J., "Effect of Variability in Fuel on Operation and Reliability of Gas Turbine," Pipeline Research Council International, 2016.

[18] Theodorus, R. and Hermanns, E., "Laminar burning velocities of methan-hydrogen air mixtures," 2007.

[19] Tay-Wo-Chong, L., Zellhuber, M., Komarek, T., Im, H. G., and Polifke, W., "Combined Influence of Strain and Heat Loss on Turbulent Premixed Flame Stabilization," *Flow, Turbulence and Combustion*, pp. 263-294, 2016.

[20] Cerutti, M., Giannini, N., Ceccherini, G., Meloni, R., Matoni, E., Romano, C. and Riccio, G., "Dry low NOx emissions operability enhancement of a heavy-duty gas turbine by means of fuel burner design development and testing," in *Asme Turbo Expo*, Oslo, Norway, 2018.

[21] Balestri, M., Cecchini, D. and Cinti, V., "Unconventional Fuels Experimental Campaigns in Gas Turbine Combustos at ENEL Sesta Facility," in *Asme Turbo Expo, GT2004-53274*, Vien, Austria, 2004.

[22] Cerutti, M., Modi, R., Kalitan, D., and Kapil, S., "Design Improvement Survey for NOx Emissions Reduction of a Heavy-Duty Gas Turbine Partially Premixed Fuel Nozzle Operating with Natural Gas: Experimental Campaign," in *Asme Turbo Expo, GT2015-43516*, Montreal, Canada, 2015.

[23] Innocenti, A., Andreini, A., Giusti, A., Facchini, B., Cerutti, M., Ceccherini, G., and Riccio, G., "Numerical Investigations of NOx Emissions of a Partially Premixed Burner for Natural Gas Operations in Industrial Gas Turbine," in *Asme Turbo Expo, GT2014-26906*, Düsseldorf, Germany, 2014.

[24] Innocenti, A., Andreini, A., Facchini, B., Cerutti, M., Ceccherini, G., and Riccio, G., "Design Improvement Survey for NO x Emissions Reduction of a Heavy-Duty Gas Turbine Partially Premixed Fuel Nozzle Operating With Natural Gas: Numerical Assessment," *Journal of Engineering for Gas Turbine and Power*, vol. 138, p. 11501, 2016.

[25] Cheolwoong Park, Changgi Kim, Young Choi, Sangyeon Won, Yasuo Moriyoshib, "The influences of hydrogen on the performance and emissioncharacteristics of a heavy duty natural gas engine," *International Journal of Hydrogen Energy*, vol. 36, no. 5, pp. 3739-3745, 2011.

[26] El Ghafour, S.A.A., El-dein, A.H.E., Aref, A.A.R., "Combustion characteristics of natural gas–hydrogen hybrid fuel turbulent diffusion flame," *International Journal of Hydrogen Energy,* vol. 35, no. 6, pp. 2556-2565, 2010.

[27] Anderson J.D., Computational Fluid Dynamics: The Basics with Applications, NJ, USA: McGrawhill Inc, 1995.

[28] Chapman, D.R., "Computational aerodynamics development and outlook.," *AIAA Journal,* 1979.

[29] Piomelli, U., "Large-eddy and direct simulation of turbulent," *VKI Lecture Notes,* 1997.

[30] Smagorinsky, J., "General circulation experiments with the primitive," *Monthly Weather Review 91,* 1963.

[31] Germano, M., Piomelli, U., Moin, P., and Cabot W.H. , "A dynamic subgrid-scale eddy viscosity model," *Physics and Fluids,* vol. 3, no. 7, 1991.

[32] J.A. van Oijen, A. Donini, R.J.M. Bastiaans, J.H.M. ten Thije Boonkkamp, L.P.H. de Goey, "State-of-the-art in premixed combustion modeling using flamelet," *Energy and Combustion Science,* vol. 57, pp. 30-74, 2016.

[33] Peters, N., "Laminar flamelet concepts in turbulent combustion," *Proc Combust Inst,* vol. 21, pp. 1231-1250, 1986.

[34] C.T. Bowman, R.K. Hanson, D.F. Davidson, W.C. Gardiner, Jr., V. Lissianski, G.P. Smith, D.M. Golden, M. Frenklach and M. Goldenberg, "http://www.me.berkeley.edu/gri_mech/," [Online].

[35] Flohr, P. and Pitsch, H., "A turbulent flame speed closure model for LES of," Center for Turbulence Research, 2000.

[36] Zimont, V. L. and Battaglia, V., "Joint RANS/LES approach to premixed flame modelling in the context of the TCF combustion model.," *Flow, Turbuulence and Combustion,* vol. 77, no. 1-4, pp. 305-331, 2006.

[37] Poinsot, T. and Veynante, D., Theoretical and Numerical Combustion, 2005.

[38] Zimont, V.L. and Lipatnikov, A.N., "A numerical model of premixed turbulent combustion of gases," *Chem. Phys. Reports,* vol. 14, no. 7, pp. 993-1025, 1995.

[39] Poinsot, T., Veynante, D., and Candel, S., "Quenching processes and premixed turbulent combustion diagrams," *Journal of Fluid Mechanics,* pp. 228-561, 1991.

[40] Müller U. C., Bollig M., Peters N., "Approximaiton for Burning Velocities and Markstein Numbers for Lean Hydrocarbon and Metanol Flames," *Combustion and Flames,* vol. 108, 1997.

[41] Sun, C.J. and Law, C.K., "On the nonlinear response of stretched premixed flames," *Combustion and Flame,* vol. 121, no. 1-2, pp. 236-248, 2000.

[42] Poinsot, T., Echekki, T., and Mungal, M.G., "A study of the laminar flame tip and implications for premixed turbulent combustion," *Combust. Sci. Technol,* vol. 81, no. 1, pp. 45-73, 1992.

[43] T. Komarek, L. Tay-Wo-Chong, M. Zellhuber, A. Huber, , and W. Polifke, "Modeling the Effect of Heat Loss on Flame Stabilization in Shear Layers," in *Int. Conf. on Jets, Wakes and Separated Flows*, Berlin, 2008.

[44] L. Tay-Wo-Chong, T. Komarek, M. Zellhuber, J. Lenz, C. Hirsch, andW. Polifke, "Influence of Strain and Heat Loss on Flame Stabilization in a Non-adiabatic Combustor," in *European Combustion Meeting*, Vienna, 2009.

[45] Tay-Wo-Chong, L., Scarpato, A., and Polifke, W., "LES Combustion Model with Stretch and Heat Loss Effects for Prediction of Premix Flame Characteristics and Dynamics," in *ASME Turbo Expo*, Charlotte, North Carolina, 2017.

[46] Nassini, P. C., Pampaloni, D., and Andreini, A., "Inclusion of Flame Stretch and Heat Loss in LES Combustion Model," in *American Institute of Physics Conference Proceedings*, 2019.

[47] Nassini, P. C, Pampaloni, D., Andreini, A., and Meloni, R.., "Large Eddy Simulation of Lean Blow-Off in a Premixed Swirl Stabilized Flame," in *Asme Turbo Expo*, Phoenix, Arizona, 2019.

[48] Bradley, D., Gaskell, P. H., Sedaghat, A., and Gu, X. J., "Generation of PDFS for Flame Curvature and for Flame Stretch Rate in Premixed Turbulent Combustion," *Combustion and Flame*, vol. 135, no. 4, pp. 503-523, 2003.

[49] Klarmann, N., Sattelmayer, T., Geng, W., and Magni, F., 2016, "Flamelet Generated Manifolds for Partially Premixed, Highly Stretched and Non-Adiabatic Combustion in Gas Turbines," in *54th AIAA Aerosp. Sci. Meet., pp. 1–14*, 2016.

[50] Meneveau, C., and Poinsot, T., "Stretching and Quenching of Flamelets in Premixed Turbulent Combustion," *Combustion and Flame*, vol. 84, no. 4, pp. 311-332, 1991.

[51] Goodwin, D. G., Speth, R. L., Moat, H. K. and Weber, B.W., "Cantera: An object-oriented software toolkit for chemical kinetics, thermodynamics, and transport processes," 2018.

[52] Pope S.B., "Ten questions concerning the large eddy simulations of turbulent flows," *New Journal of Physics*, vol. 6, 2004.

[53] Pope S.B., "Turbulent Flows," *Cambridge University Press*, 2011.

[54] ANSYS, "Fluent 16 Theory Guide," 2014.

[55] Lefebvre, A.H. and Ballal, D.R., Gas Turbine Combustion, Taylor & Francis, 2010.

[56] Bilger, R.W. and Beck, R.E., "15th Symp. (Int'l.) on Combustion, pp.541," in *The Combustion Institute*, 1975.

[57] Nassini, P. C., Pampaloni, D., and Andreini, A., "Impact of Stretch and Heat Loss on Flame Stabilization in a Lean Premixed Flame Approaching Blow-Off," in *Energy procedia, pp.250-257*, 2018.

[58] Pampaloni, D., Andreini, A., Facchini, B. and Paschereit, C. O. , "LES modelling of the flame describing function of a lean premixed swirl stabilized flame," *Journal of Propulsion and Power*, p. 4608, 2018.